Title

Inhomogeneous primordial nucleosynthesis: Coupled nuclear reactions and hydrodynamic dissipation processes

Journal

Astrophysical Journal, 423(1)

ISSN

0004-637X

Authors

Jedamzik, K
Fuller, GM
Mathews, GJ

Publication Date

1994-03-01

DOI

10.1086/173789

Peer reviewed

THE ASTROPHYSICAL JOURNAL, 423:50–67, 1994 March 1

INHOMOGENEOUS PRIMORDIAL NUCLEOSYNTHESIS: COUPLED NUCLEAR REACTIONS AND HYDRODYNAMIC DISSIPATION PROCESSES

KARSTEN JEDAMZIK[1] AND GEORGE M. FULLER
Department of Physics, University of California, San Diego, La Jolla, CA 92093-0319
AND
GRANT J. MATHEWS
University of California, Lawrence Livermore National Laboratory, Livermore, CA 94550
Received 1993 June 21; accepted 1993 August 30

ABSTRACT

We present a detailed numerical study of inhomogeneous big bang nucleosynthesis where, for the first time, nuclear reactions are coupled to all significant fluctuation dissipation processes. These processes include neutrino heat transport, baryon diffusion, photon diffusive heat transport, and hydrodynamic expansion with photon-electron Thomson drag. Light-element abundance yields are presented for broad ranges of initial amplitudes and length scales for spherically condensed fluctuations. The ^{2}H, ^{3}He, ^{4}He, and ^{7}Li nucleosynthesis yields are found to be inconsistent with observationally inferred primordial abundances for all but very narrow ranges of fluctuation characteristics. Rapid hydrodynamic expansion of fluctuations late in the nucleosynthesis epoch results in significant destruction of ^{7}Li (^{7}Be) only if the baryonic contribution to the closure density (Ω_b) is less than or comparable to the upper limit on this quantity from homogeneous big bang nucleosynthesis. This implies that ^{7}Li overproduction will preclude an increase on the upperlimit for Ω_b for any inhomogeneous nucleosynthesis scenario employing spherically condensed fluctuations.

Subject headings: early universe — hydrodynamics — nuclear reactions, nucleosynthesis, abundances

1. INTRODUCTION

In this work we study the primordial nucleosynthesis process in the presence of nonlinear subhorizon-scale baryon-to-photon number ratio fluctuations. Our study is unique in that we couple all relevant hydrodynamic dissipation processes to nuclear reactions. It is our goal to further the understanding of big bang nucleosynthesis to the point where it can be used to probe the fluctuation-generation physics of the very early universe.

Homogeneous standard big bang nucleosynthesis (hereafter HBBN; Wagoner, Fowler, & Hoyle 1967; Wagoner 1973) has become one of the most important and successful tools for constraining the physics of the early universe (cf. Schramm & Wagoner 1977; Yang et al. 1984; Walker et al. 1991; Smith, Kawano, & Malaney 1993; Malaney & Mathews 1993; see also the discussion in Kolb & Turner 1990). Comparison of light-element nucleosynthesis yields with observationally inferred primordial abundances allows limits to be placed on the baryon-to-photon ratio (η) and the expansion rate of the universe and, hence, the energy density during the nucleosynthesis epoch. One of the key assumptions of HBBN is that η is homogeneously distributed.

By contrast, in inhomogeneous standard big bang nucleosynthesis (IBBN) the assumption of a homogeneous spatial distribution of η is relaxed. In studies of IBBN the object is to calculate primordial nucleosynthesis abundance yields associated with a given spectrum of fluctuations in baryon-to-photon number ratio extant at the nucleosynthesis epoch. If this can be done with confidence, then the usefulness of big bang nucleosynthesis for constraining the physics of the early universe can be extended. In particular, any process which generates fluctuations prior to the nucleosynthesis epoch may be subject to constraint. Possible fluctuation-generation processes associated with the QCD epoch, the electroweak transition, and topological defects among others are discussed in Malaney & Mathews (1993). Nonlinear fluctuations on small spatial scales which could affect primordial nucleosynthesis may even be produced in an inflationary epoch (Yokoyama & Suto 1991; Dolgov & Silk 1992).

The hydrodynamic evolution of fluctuation characteristics from production at very early times ($T \lesssim 100$ GeV) through the nucleosynthesis epoch ($T \approx 1$ keV) is discussed in Heckler & Hogan (1993) and Jedamzik & Fuller (1994, hereafter JF94). In the present study we add to that work a calculation of the light-element nucleosynthesis yields associated with the fluctuation evolution.

The calculation of primordial nucleosynthesis yields in inhomogeneous conditions has received extensive previous treatment (e.g., Epstein & Petrosian 1975; Applegate, Hogan, & Scherrer 1987; Alcock, Fuller, & Mathews 1987; Malaney & Fowler 1988; Fuller, Mathews, & Alcock 1988; Terasawa & Sato 1989a, b, c, 1990; Kurki-Suonio & Matzner 1989, 1990; Kurki-Suonio et al. 1988, 1990; Mathews et al. 1990; Thomas et al. 1994). These and other IBBN calculations are reviewed in Malaney & Mathews (1993). A vexing problem in computing IBBN abundance yields is that dissipative processes which modify fluctuation characteristics can proceed on timescales which are comparable to or shorter than nuclear reaction timescales. The fluctuation damping processes which can be important in the epoch between $T \approx 1$ MeV and $T \approx 1$ keV are baryon diffusion, photon diffusive heat transport, and hydrodynamic expansion. In fact, even the most sophisticated of the calculations listed above neglect all fluctuation dissipation processes except for baryon diffusion.

Neglect of photon diffusion and hydrodynamic expansion in previous IBBN work has left considerable uncertainty in the nuclear abundance yields to be expected from given fluctuation characteristics. Alcock et al. (1990) showed that the rapid

[1] Present address: University of California, Lawrence Livermore National Laboratory, Livermore, CA 94550.

hydrodynamic expansion of fluctuations that sets in after $e^{\pm}$ pair annihilation conceivably could result in changes in the ^{2}H and ^{4}He yields and, in particular, in destruction of ^{7}Li by orders of magnitude. This uncertainty in ^{7}Li production has diminished the usefulness of IBBN as a constraint on primordial inhomogeneity.

In this paper we present the results of IBBN calculations which, for the first time, couple nuclear reactions with photon diffusion, hydrodynamic expansion, and neutron, proton, and ion diffusion. We also include neutrino heat conduction which modifies fluctuations prior to the nucleosynthesis epoch. Nucleosynthesis yields are computed for broad ranges of initial characteristics. These calculations allow us to predict confidently the ^{2}H, ^{3}He, ^{4}He, and ^{7}Li abundances to be expected for particular fluctuation configurations.

In § 2 we describe how fluctuations are modeled and numerically evolved through the nucleosynthesis epoch. In particular, we discuss how fluctuation damping processes are coupled with nuclear reactions in a multi–spatial-zone calculation. Section 3 presents the results of our numerical computations of nucleosynthesis yields. Conclusions are given in § 4.

2. NUMERICAL FLUCTUATION EVOLUTION AND NUCLEOSYNTHESIS CALCULATIONS

We numerically evolve spherically condensed fluctuations from $T = 100$ MeV through the end of the nucleosynthesis era at about $T \approx 1$ keV. Initial fluctuation characteristics are specified at the epoch where $T = 100$ MeV. We consider fluctuations in baryon-to-photon number ratio. These are equivalent to fluctuations in the entropy per baryon as discussed in JF94. We will adopt the notation of that paper here. The amplitude of a fluctuation in η at a position x is defined in terms of the average net baryon number density in the horizon, $\bar{n}_b$, and the appropriate baryonic density $n_i(x)$, as

$$\Delta_i(x) = \frac{n_i(x)}{\bar{n}_b} . \tag{1}$$

This expression represents the amplitude for fluctuations in protons or neutrons when the subscript i is replaced by p or n, respectively. Fluctuation amplitudes in light-element number density are denoted in a similar fashion. For example, the spatial distribution of the ^{4}He overdensity is described by $\Delta_{^4\mathrm{He}}(x)$. If $\Delta(x)$ has no subscript, it is understood to represent the fluctuation amplitude in total net baryon number density at position x.

We assume that the horizon volume at $T = 100$ MeV is filled with a regular lattice of identical spherical cells, each of which has a Gaussian-shape fluctuation at its center. Although this is certainly an idealization, the anticorrelated domains expected from, for example, a homogeneous nucleation of phase should approximate a regular lattice. Meyer et al. (1991) have studied the changes in IBBN abundance yields to be expected for a distribution of fluctuation centers arising from a realistic nucleation process. In that work the more realistic distributions give slight increases in the ^{4}He abundance yields. Our calculated abundance yields should be similarly modified where appropriate. A Gaussian shape is a good form to use, since baryon diffusion tends to evolve fluctuations to a Gaussian shape, independently of their initial profile.

We refer proper lengths to a comoving scale at $T = 100$ MeV. Consider a length scale comoving with the Hubble expansion which has proper length L at an epoch where the temperature is T and the scale factor is $R(T)$. The "comoving" length associated with this length scale L is defined to be L_{100},

$$L_{100} = L\left[\frac{R_{100}}{R(T)}\right], \tag{2}$$

where R_{100} is the scale factor for the universe at the epoch where $T = 100$ MeV. In what follows we set $R_{100} = 1$.

The initial distribution of baryons in the horizon is specified by giving three fluctuation characteristics: the amplitudes, the Gaussian width, and the radius of the spherical fluctuation cell. Figure 1 shows a schematic representation of our fluctuation distribution. In this figure we plot $\log_{10} \Delta(x)$ against position. The Gaussian width of the fluctuations is $2a_{100}$. The radius of a spherical fluctuation cell is l^s_{100}, so that the mean separation between fluctuation centers is approximately $2l^s_{100}$. In our numerical calculations we characterize the initial amplitude of the distribution $\Delta(x)$ in a fluctuation cell by the ratio

$$\Lambda \equiv \frac{\Delta\ (\mathrm{center})}{\Delta\ (\mathrm{edge})} , \tag{3}$$

where Δ (center) represents the value of Δ at the peak of the

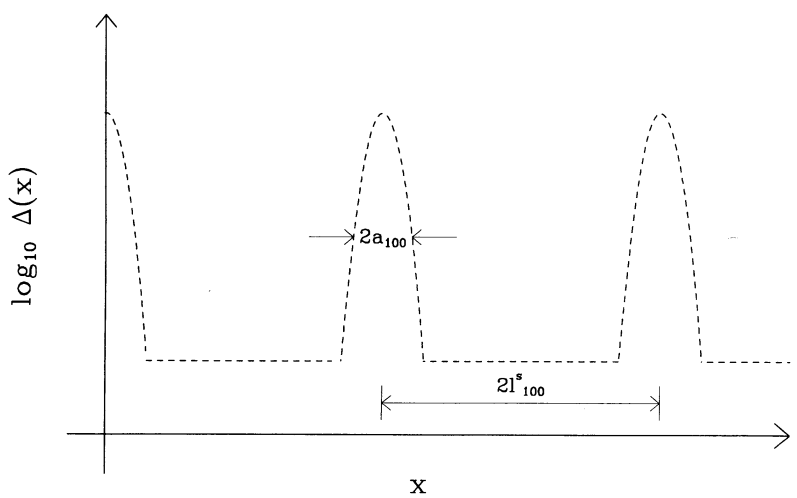

FIG. 1.—Schematic representation of fluctuation amplitude $\Delta(x)$ plotted against position x. Initial fluctuation separation $2l^s_{100}$ and width $2a_{100}$ are shown.

Gaussian distribution and Δ (edge) represents the minimum value of Δ on the edge of a spherical cell. Thus Λ is a measure of the density contrast between high- and low-density regions of a spherical cell volume. With these definitions the initial baryon number distribution, for $\Lambda \gg 1$, is

$$\Delta(x_{100}) \approx A\{\Lambda \exp [-(x_{100}/a_{100})^2] + 1\} , \quad (4a)$$

where x_{100} is the comoving radial coordinate and A is a normalization constant determined by

$$4\pi \int_0^{l_{100}} x_{100}^2 \Delta(x_{100}) dx_{100} = 1 . \quad (4b)$$

In equation (4a) we have assumed that $\Lambda \gg 1$, but in our numerical calculations we consider the general case.

Our computations follow the evolution of only one spherical fluctuation cell. We employ reflective boundary conditions at the edge of the spherical cell for all diffusive and hydrodynamic flows. Reflective boundary conditions are appropriate in the limit where the fluctuation cells form a regular lattice (cf. Fig. 1).

We divide a spherical fluctuation cell into 24 spatial zones. We solve for the hydrodynamic evolution of the fluctuation cell in the manner described in JF94, but with special modifications for treating coupled nuclear reactions and photon dissipative processes. Bayons, ions, and heat are transported between zones by radiative conduction of neutrinos and photons, diffusion, and hydrodynamic flows. We also follow the annihilation of $e^{\pm}$ pairs in detail. However, the effects of muon and pion annihilation are neglected in these computations. This approximation is justified in the discussion in JF94.

Nuclear abundances and the energy density in each zone can be modified by nuclear reactions. We include the effects of nuclear reactions in our evolution calculations by solving a reaction network in each spatial zone. The reaction network in each zone is coupled to the nuclear evolution in the other zones through baryon and ion diffusion and hydrodynamic processes. Nuclear reactions in each zone are followed in a manner similar to that of the Wagoner et al. (1967; also Wagoner 1973) code as updated by Kawano (1992). The reaction network in our calculation includes nuclei up to and including mass $A = 12$. The reaction rates employed are somewhat modified from the Smith et al. (1993) study and are discussed in § 3.

As in Wagoner et al. (1967), we employ a second-order Runge-Kutta driver to follow the time evolution of the nuclear abundances y_i^k (i = nuclide index; k = zone index), the scale factor R, and the cosmic average temperature T. The y_i^k are number fractions of nuclear species i relative to hydrogen (protons) in zone k. In the Runge-Kutta algorithm, changes in nuclear abundances and thermodynamic quantities are computed twice and averaged for each time step.

We employ a fully implicit differencing scheme for the simultaneous coupling of nuclear reactions and neutron diffusion. In this scheme we invert a matrix of nuclear reaction rates and zone-to-zone neutron diffusion rates for each time step. Neutron diffusion and nuclear reactions must be coupled completely implicitly in order to follow the nuclear evolution of high-amplitude fluctuations. This is because nuclear reaction and neutron diffusion timescales can become comparable for these fluctuations. Neutron diffusion rates for smaller amplitude fluctuations are usually not as fast as typical nuclear reaction rates. A coupling scheme for high-amplitude fluctuations which employs only a partially implicit algorithm requires decreasing time steps. This may result in a time-step crash. In our calculations we find that an explicit coupling of proton and ion diffusion with nuclear reactions is sufficient to follow the evolution of nuclear abundances accurately.

Photon diffusive heat transport, hydrodynamic expansion with radiation drag, and nuclear reactions are adequately modeled with an explicit coupling in our numerical computations. The physics of fluctuation modification by photon diffusion and hydrodynamic expansion is studied in JF94. In that work it is shown that a key quantity for determining the efficacy of these processes is the photon mean free path $l_\gamma(x, t)$. Photons can be either optically thick or optically thin across a spatial zone, according to whether $l_\gamma(x, t)$ (evaluated at the zone center) is smaller than or larger than the zone size.

Our numerical calculations employ a diffusive photon heat transport scheme when photons are optically thick. Zones coupled in this manner are well approximated as being in pressure equilibrium with each other. The effects of photon diffusive heat transport during a time step are modeled by expansion or contraction of individual zones to obtain a new pressure equilibrium. In this manner zones evolve through a succession of pressure equilibrium states. This scheme will be accurate as long as the sound crossing time is short compared with the photon diffusive heat transport time between zones. We employ a Lagrangian grid to facilitate the modeling of expansion or contraction of individual zones.

In the limit where photons are optically thin, the approximation of pressure equilibrium between zones breaks down. In this case pressure gradients result in local acceleration of fluid elements. Fluid velocities rapidly obtain terminal velocities due to photon-electron Thomson drag (Alcock et al. 1990; JF94). In our IBBN calculations we neglect acceleration times and treat terminal velocities as being attained instantaneously. We determine terminal fluid velocities by balancing local pressure-gradient–induced hydrodynamic stresses against radiation drag forces. In our calculations hydrodynamic expansion is modeled with an Eulerian grid which allows for fluid motions across zone boundaries.

In the calculations of fluctuation evolution it is common to encounter a situation in which the high-density central zones are optically thick to photons, while the low-density outer zones are optically thin. An exact treatment of the momentum transfer between baryons and photons in this case would require a solution of the Boltzmann equation. In this study we approximate the transition between optically thick and optically thin transport regimes by using a superposition of the techniques outlined above for the two limiting cases.

We introduce an independent set of "photon zones." These zones are required to be larger than the photon mean free path at any point and time. The photon zones and baryon zones are taken to be initially coincident at $T = 100$ MeV. For lower temperatures the photon mean free path can grow rapidly, especially during the $e^{\pm}$ pair annihilation epoch. This necessitates employing a rezoning procedure to produce increasingly larger photon zones. Eventually photon zones and baryon zones are not coincident. For example, one photon zone could include a cluster of baryon zones, each having different baryon content and nuclear abundances but the same photon temperature. In regimes where rapid hydrodynamic expansion occurs, the entropy generation due to radiation drag is rapid enough to justify an assumption of uniform photon, electron, and baryon temperature.

Where baryon and photon zones are not coincident, the

numerical procedures for computing fluid velocities and pressure equilibrium conditions must be chosen carefully in order to avoid time-step and spatial instabilities. In our IBBN calculations local fluid velocities are determined by an effective pressure gradient between adjacent baryon zones. This effective pressure gradient includes contributions from gradients in effective photon temperature as well as from gradients in neutron, proton, ion, and electron pressures. In the case where photon zones contain many baryon zones, we assign effective photon temperatures to each baryon zone. These effective temperatures are assigned by interpolating between photon temperatures in adjacent photon zones. In this procedure we allow for fluid movements across common baryon and photon zone boundaries.

We employ a three-step algorithm for computing the effects of fluid flow, heat transport, and radiation drag on fluctuation evolution. First we compute changes in energy density in photon zones arising from photon heat diffusion. This causes deviations from pressure equilibrium between photon zones. In the second step we compute the effects of local effective pressure gradients and associated fluid movements across baryon zone boundaries. Finally, we expand or contract baryon and photon zones to achieve pressure equilibrium where appropriate.

In order to obtain optimal convergence in nucleosynthesis yields, we place most of the baryon zones where the baryon number gradients are largest. Figure 2 displays the average abundance yields in ^{4}He (*solid line*) and ^{7}Li (*dashed line*) as a function of number of baryon zones employed in a particular calculation. This calculation evolved a fluctuation which was taken to have large initial density contrast ($\Lambda = 1.25 \times 10^6$) Convergence for such high-amplitude fluctuations is problematic due to the pronounced effects of hydrodynamic damping. In this investigation we use 24 baryon zones, implying intrinsic computational uncertainties in the nucleosynthesis yields of $\Delta Y_p/Y_p \sim 1\%$, $\Delta y_{2H}/y_{2H} \sim 10\%$, and $\Delta y_{7Li}/y_{7Li} \sim 20\%$. Here y_{2H} and y_{7Li} denote number fractions relative to hydrogen, while Y_p represents the primordial ^{4}He mass fraction.

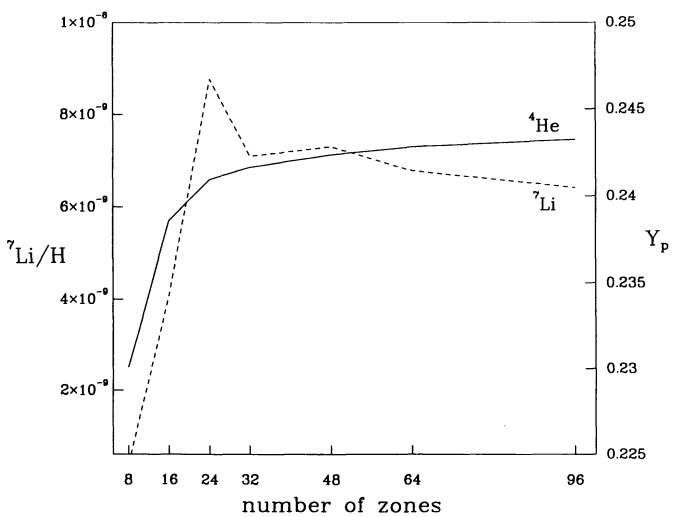

FIG. 2.—Plot of the computed ^{7}Li/H ratio (*dashed line*) and ^{4}He mass fraction Y_p (*solid line*) against the number of baryon zones employed in the calculation. Results on this plot are for a fluctuation with $\Lambda = 1.25 \times 10^6$, $a_{100} = 0.5$ m, and $l^s_{100} = 10$ m. For this set of calculations we take $\Omega_b = 0.025$ h^{-2}.

3. RESULTS OF INHOMOGENEOUS BIG BANG NUCLEOSYNTHESIS CALCULATIONS

In this section we discuss the nucleosynthesis yields obtained with our coupled nuclear reaction and hydrodynamic damping simulations. In general, our calculated average nucleosynthesis yields agree well with those obtained by Kurki-Suonio & Matzner (1989, 1990), Kurki-Suonio et al. (1988, 1990), Terasawa & Sato (1989a, b, c), and Mathews et al. (1990) when the fluctuations considered are relatively low in initial density contrast (Λ) and have large initial volume filling fractions (i.e., small l^s_{100}/a_{100}). This is not surprising, since we would expect photon diffusive effects and hydrodynamic damping to be minimal for fluctuations with these characteristics. By contrast, our results for fluctuations with high Λ and large l^s_{100}/a_{100} can differ significantly from previous studies. We therefore concentrate the discussion here on the nucleosynthesis yields obtained from fluctuations with larger values for Λ and l^s_{100}/a_{100}. We also consider a wider range in the fractional contribution of baryons to the closure density (Ω_b) than do previous IBBN studies.

Figures 3–7 show the fluctuation amplitude (Δ_i) as a function of cell radius r_{100} for protons (*solid line*), neutrons (*dotted line*), ^{2}H (*long-dashed line*), ^{3}He (*short-dash–dot line*), ^{4}He (*short-dashed line*), ^{7}Li (*long-dash–dot line*), and ^{7}Be (*short-dashed line*). Confusion between the short-dashed lines for ^{4}He and ^{7}Be can be avoided by noting that the abundance of ^{4}He is always orders of magnitude larger than that for ^{7}Be. The total ^{7}Li yield long after the nucleosynthesis epoch is the sum of the ^{7}Li and ^{7}Be abundances shown on these plots. Each figure is labeled by the initial values of Λ, l^s_{100}, and l^s_{100}/a_{100}, and the overall average Ω_b used in the calculation. In the expressions for the baryonic contribution to the closure density, h is the value of the Hubble parameter in units of 100 km s^{-1} Mpc^{-1}. The upper limit on Ω_b from homogeneous primordial nucleosynthesis is $\Omega_b \approx 0.013\ h^{-2}$.

Figure 3 shows nine "snapshots" in the evolution of a fluctuation with initial characteristics $\Lambda = 3 \times 10^7$, $l^s_{100} = 0.5$ m, and $l^s_{100}/a_{100} = 25$. We use an overall average baryonic density of $\Omega_b = 0.025\ h^{-2}$ in this calculation. The snapshots correspond to epochs with temperatures (in MeV) $T = 100$, 5.0, 2.5, 1.0, 0.25, 0.10, 0.05, 0.025, 0.01. Figures 4–7 show snapshots in the nucleosynthesis yields and fluctuation amplitude evolution for different initial fluctuation parameters and values of Ω_b. In these figures the snapshots correspond to epochs with temperatures (in MeV) $T = 100$, 1.0, 0.25, 0.10, 0.075, 0.050, 0.025, 0.01, 0.008. Figure 4 shows the evolution of a fluctuation with initial characteristics $\Lambda = 3 \times 10^7$, $l^s_{100} = 50$ m, and $l^s_{100}/a_{100} = 25$. This evolution sequence is computed with an overall average $\Omega_b = 0.25\ h^{-2}$. Figure 5 is the same as Figure 4, but with $\Omega_b = 0.0125\ h^{-2}$ and with initial fluctuation characteristics $\Lambda = 1.25 \times 10^6$, $l^s_{100} = 14$ m, and $l^s_{100}/a_{100} = 20$. Figure 6 is similar to Figure 4, but with parameters $\Omega_b = 0.25\ h^{-2}$, $\Lambda = 2 \times 10^9$, $l^s_{100} = 50$ m, and $l^s_{100}/a_{100} = 100$. Similarly, Figure 7 shows the fluctuation evolution for parameters $\Omega_b = 0.0083\ h^{-2}$, $\Lambda = 1.25 \times 10^7$, $l^s_{100} = 50$ m, and $l^s_{100}/a_{100} = 1000$. Figures 6 and 7 show the various fluctuation amplitude profiles only for the core regions of the fluctuation cells.

Average nuclear abundance yields computed for a variety of initial fluctuation characteristics and overall average values of Ω_b are given in Figures 8–14.

Figures 8, 10, 12, and 14 show average nucleosynthesis yields of ^{4}He, ^{7}Be (unstable), ^{7}Li, ^{2}H, ^{3}He (unstable) as a function

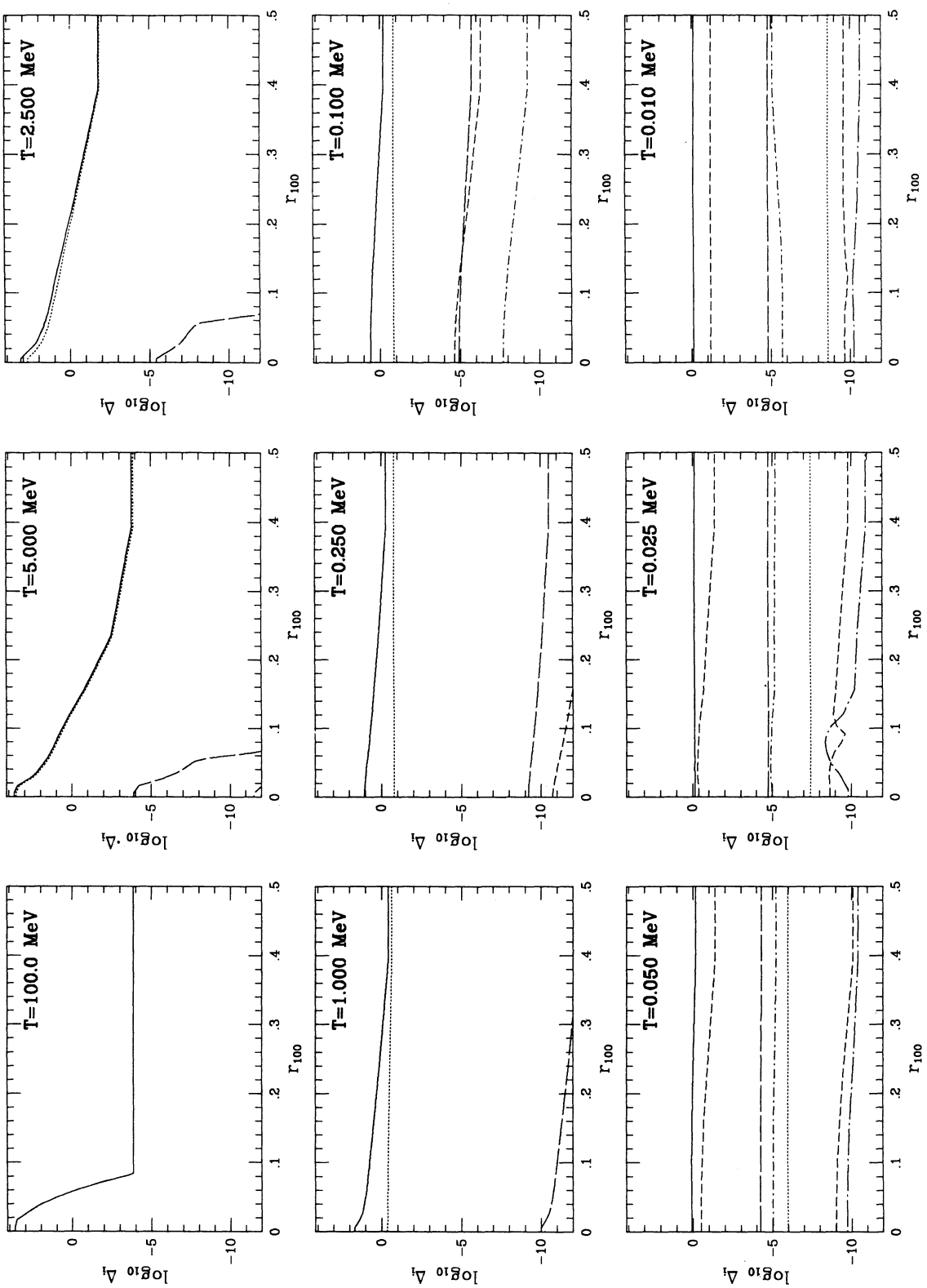

Ω_b=0.025h^{-2}, l^s_{100}=0.5m, l^s_{100}/a_{100}=25, Λ=3×10^7

FIG. 3.—Plots of the fluctuation amplitude $\log_{10} \Delta_i$ as a function of cell radius r_{100} for protons (*solid line*), ^{2}H (*long-dashed line*), ^{3}He (*short-dash–dot line*), ^{4}He (*short-dashed line*), ^{7}Li (*long-dash–dot line*), and ^{7}Be (*short-dashed line*). Note that the fluctuation amplitude for ^{4}He is orders of magnitude larger than that for ^{7}Be. Shown are $\log_{10} \Delta_i$ profiles at epochs (T/MeV) = 100, 5, 2.5, 1.0, 0.25, 0.10, 0.05, 0.025, 0.01. An overall average $\Omega_b = 0.025\,h^{-2}$ was used in this calculation. The initial fluctuation characteristics asumed for this calculation are $\Lambda = 3 \times 10^7$, $l^s_{100} = 0.5$ m, and $l^s_{100}/a_{100} = 25$.

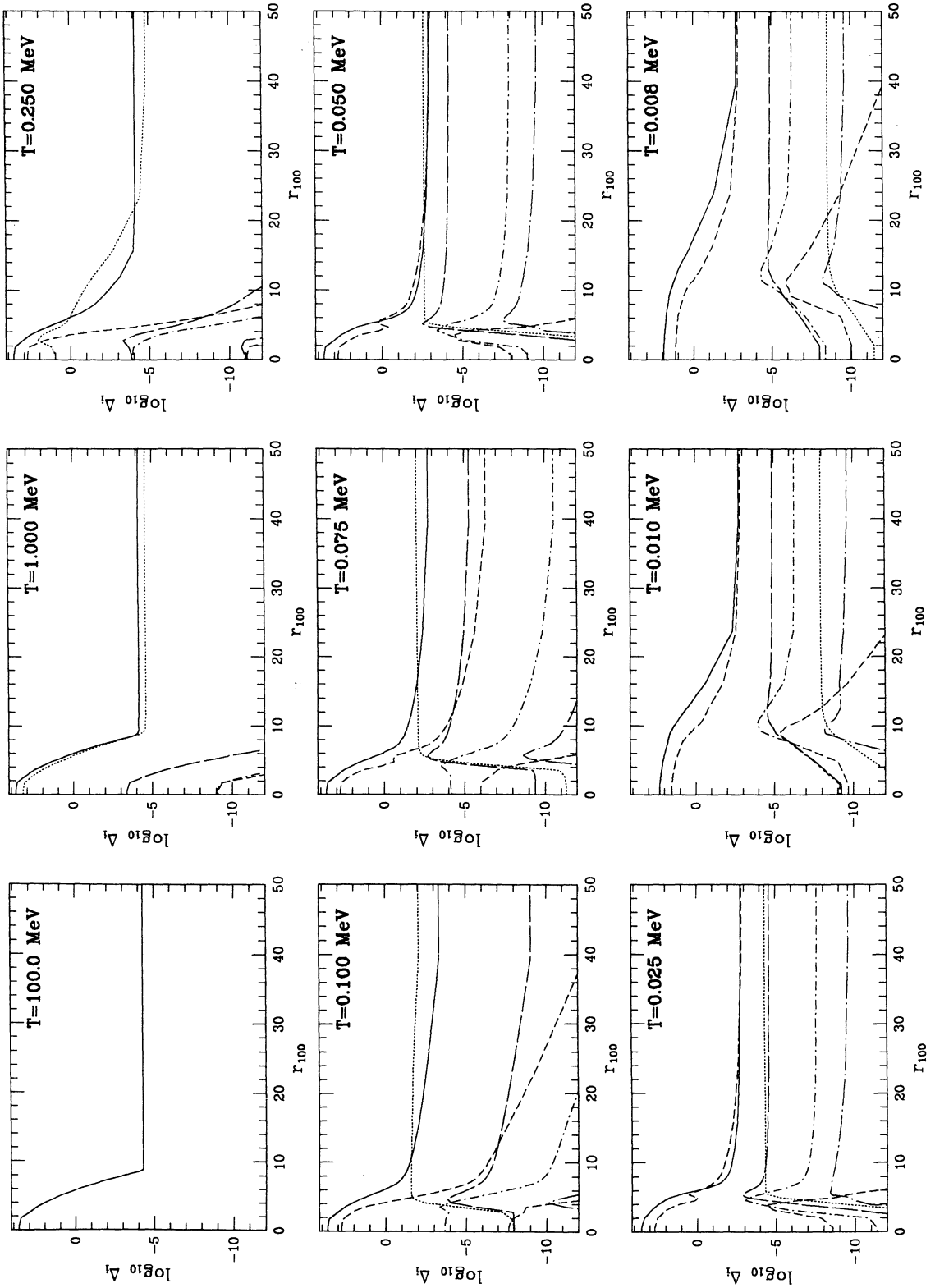

Ω_b=0.25h^{-2}, l^s_{100}=50m, l^s_{100}/a_{100}=25, Λ=3×10^7

FIG. 4.—Similar to Fig. 3, but with $\Omega_b = 0.25\ h^{-2}$ and initial fluctuation parameters $\Lambda = 3 \times 10^7$, $l^s_{100} = 50$ m, and $l^s_{100}/a_{100} = 25$. In this plot $\log_{10} \Delta_i$ profiles are given at epochs (T/MeV) = 100, 1.0, 0.25, 0.10, 0.075, 0.050, 0.025, 0.01, 0.008.

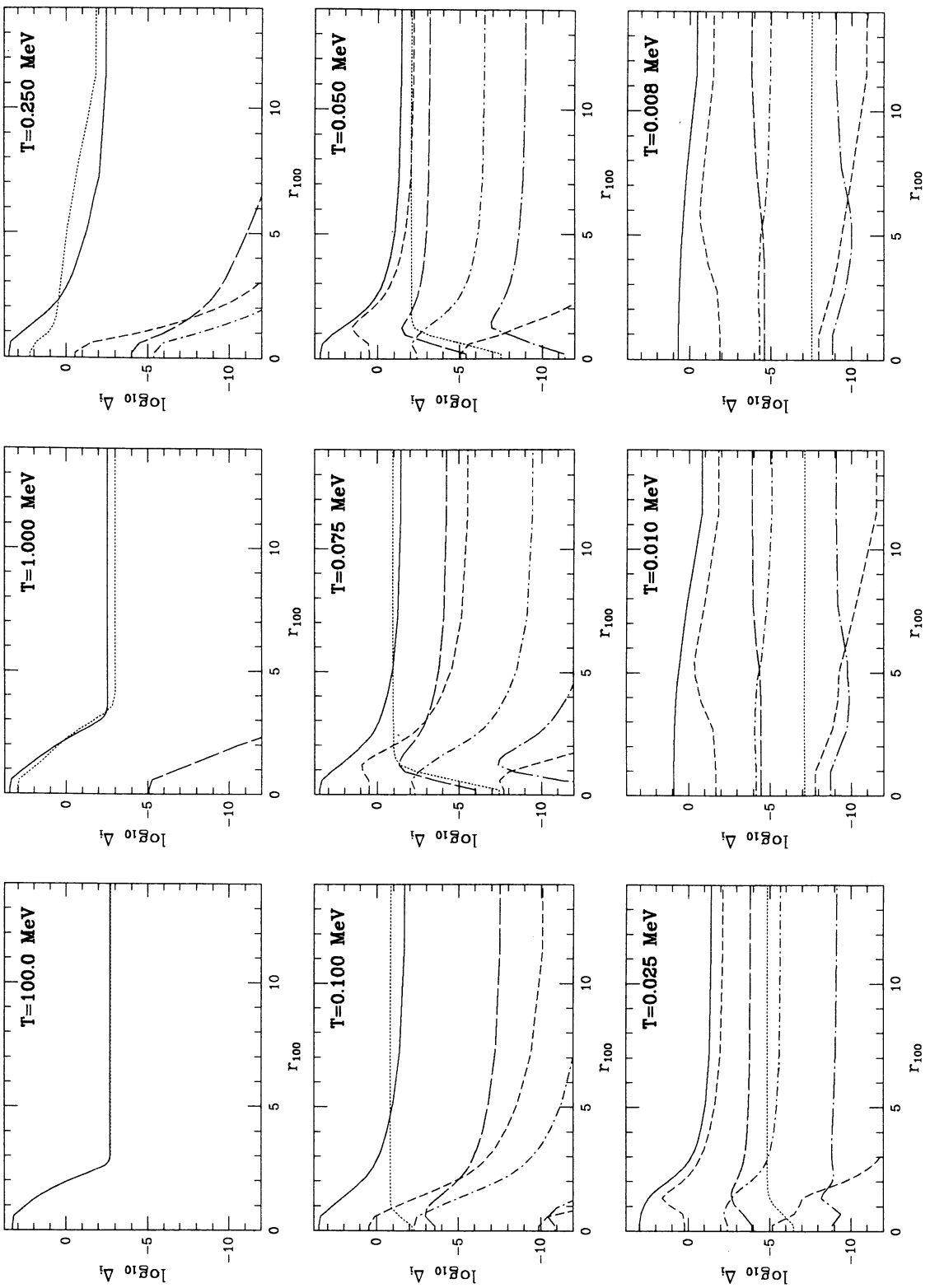

$\Omega_b = 0.0125h^{-2}$, $l^s_{100} = 14\text{m}$, $l^s_{100}/a_{100} = 20$, $\Lambda = 1.25 \times 10^6$

FIG. 5.—Same as Fig. 4, but with parameters $\Omega_b = 0.0125\,h^{-2}$, $\Lambda = 1.25 \times 10^6$, $l^s_{100} = 14$ m, and $l^s_{100}/a_{100} = 20$.

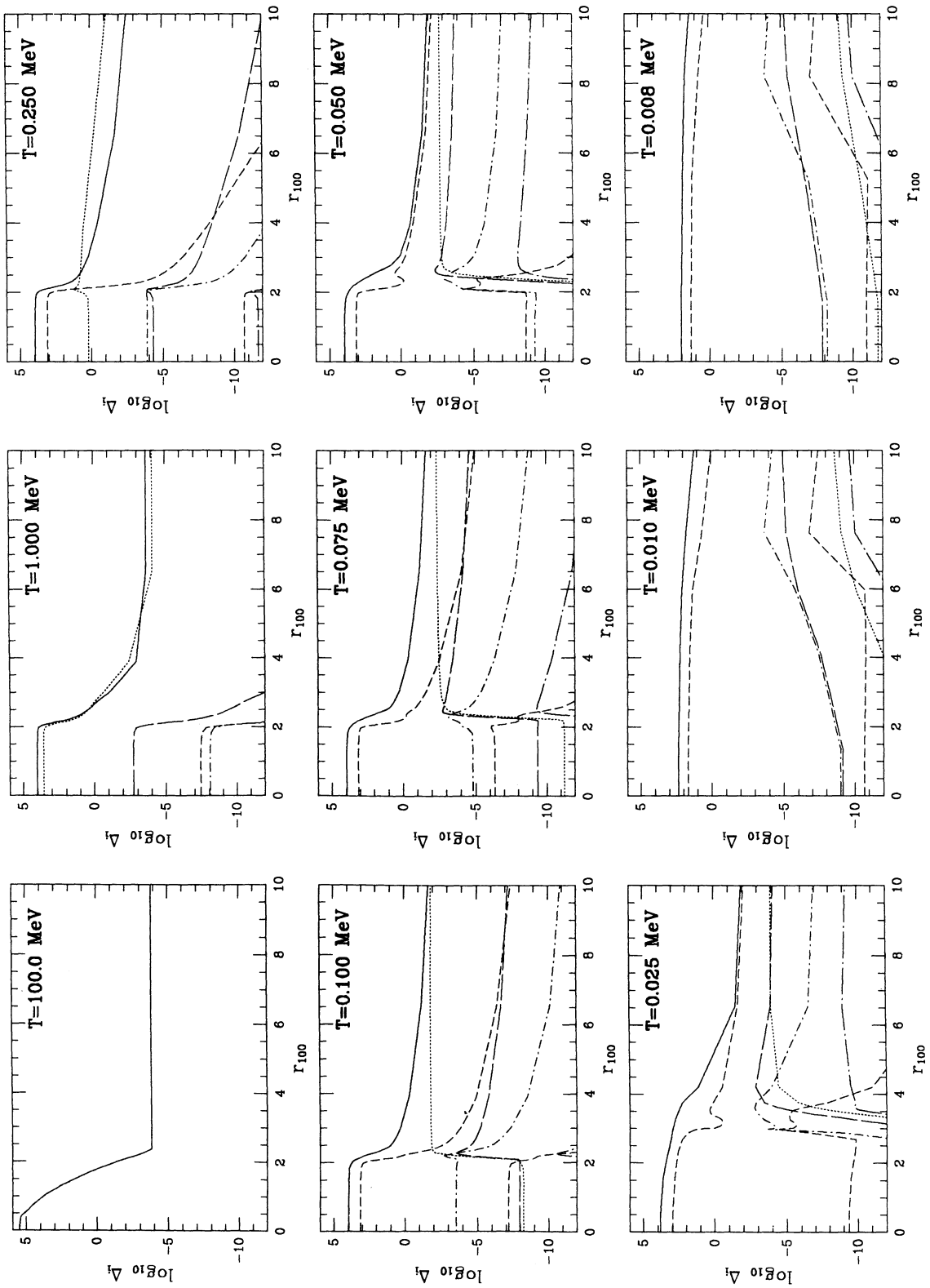

FIG. 6.—Same as Fig. 4, but with parameters $\Omega_b = 0.25\,h^{-2}$, $\Lambda = 2 \times 10^9$, $l^s_{100} = 50$ m, and $l^s_{100}/a_{100} = 100$. In this figure $\log_{10} \Delta_i$ profiles are given for the fluctuation core region ($r_{100} \leq 10$ m) only.

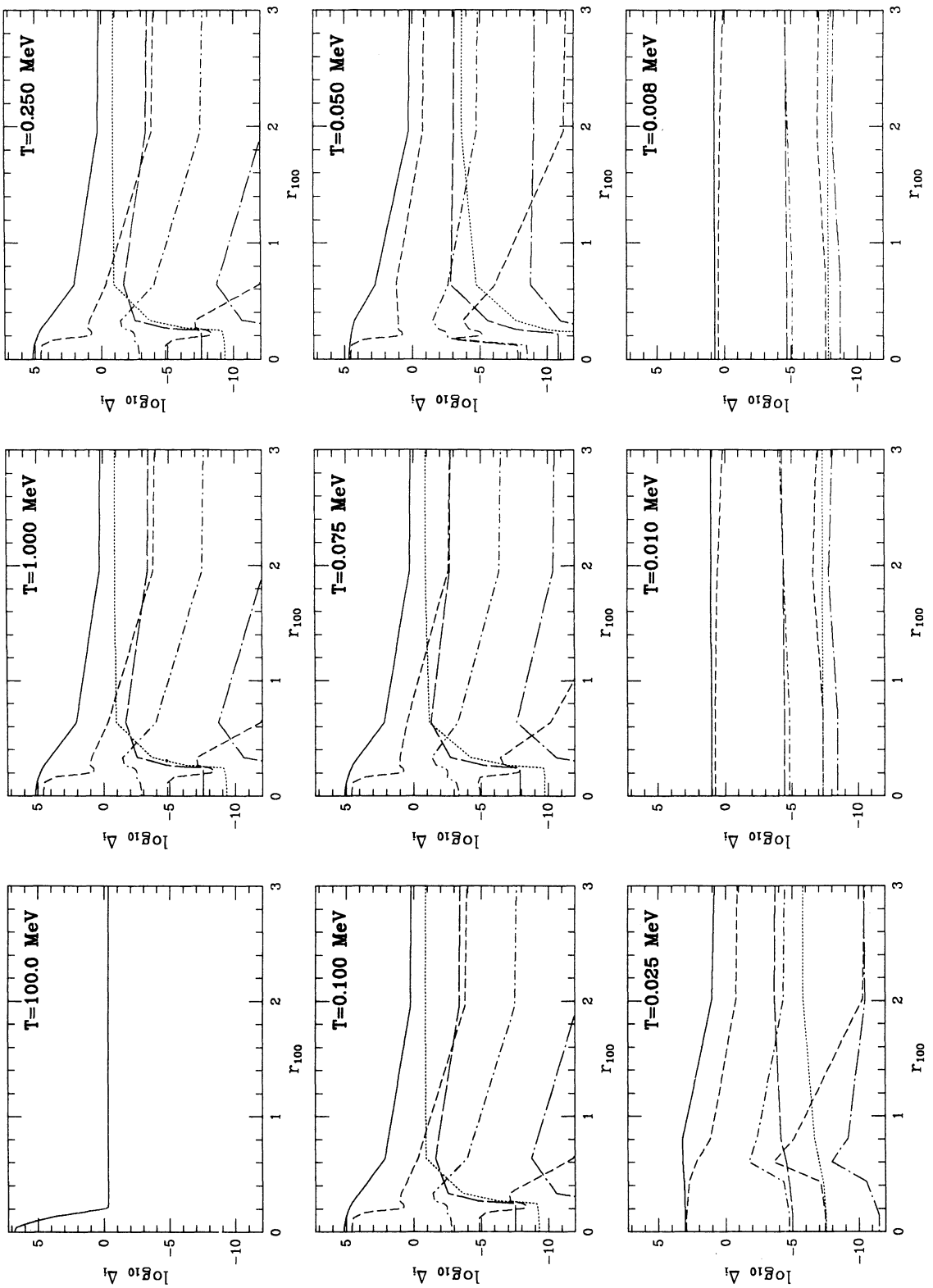

FIG. 7.—Same as Fig. 6, but with parameters $\Omega_b = 0.0083\,h^{-2}$, $\Lambda = 1.25 \times 10^7$, $l^s_{100} = 50$ m, and $l^s_{100}/a_{100} = 1000$. The $\log_{10} \Delta_i$ profiles are shown for fluctuation core region ($r_{100} \leq 3$ m) only.

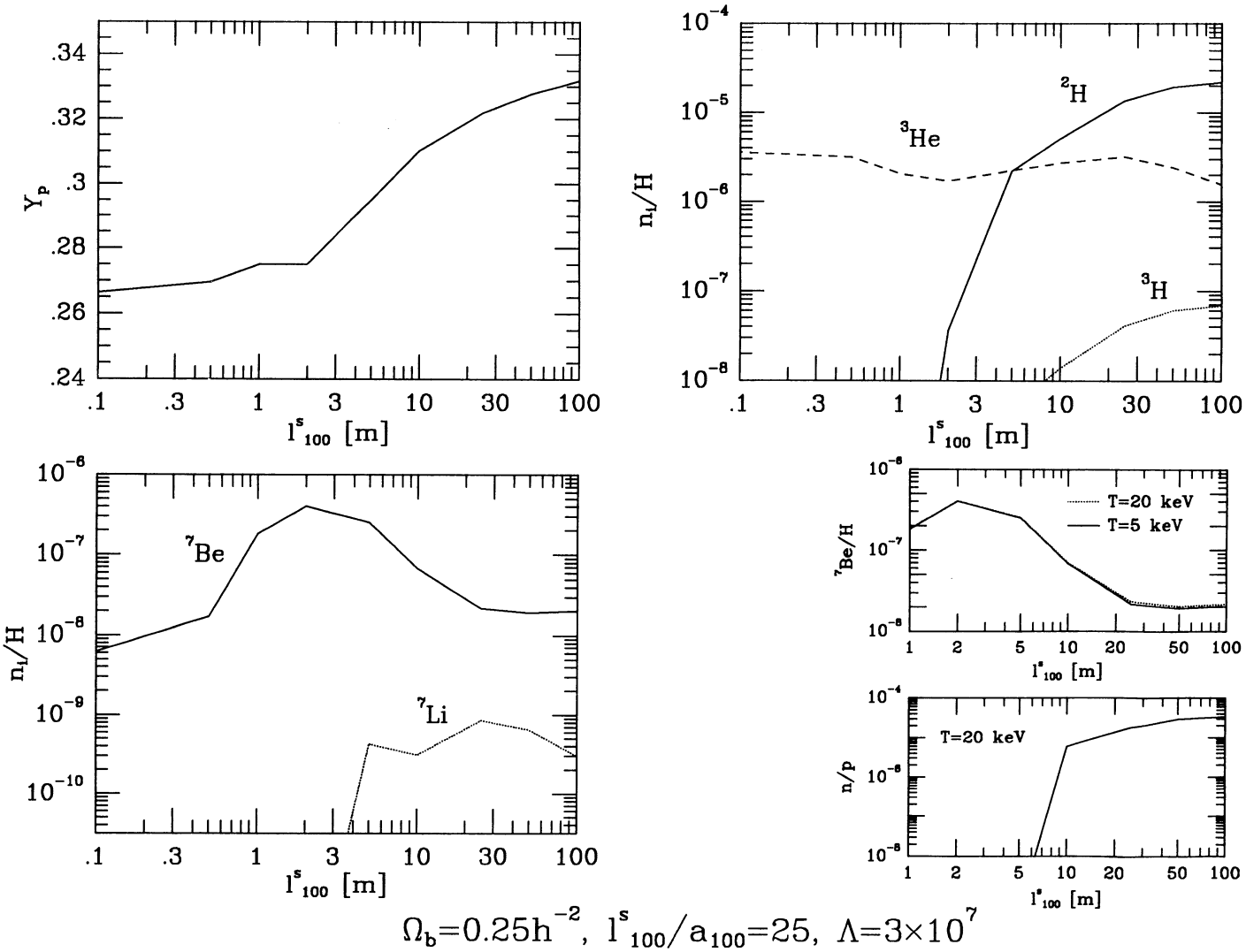

FIG. 8.—Average nucleosynthesis yields are shown as a function of initial fluctuation cell radius l^s_{100} in meters. The upper left-hand panel gives the ^{4}He mass fraction Y_p, while the lower left-hand and upper right-hand panels give number fractions relative to hydrogen for ^{7}Be, ^{7}Li, ^{3}He, ^{2}H, and ^{3}H as indicated. The two lower right-hand plots give the average ^{7}Be/H ratios (at $T = 20$ keV and $T = 5$ keV) and the average neutron-to-proton ratio (at $T = 20$ keV) as a function of l^s_{100}. These calculations were performed for fixed $\Lambda = 3 \times 10^7$ and $l^s_{100}/a_{100} = 25$, and assume an average $\Omega_b = 0.25\,h^{-2}$.

of fluctuation cell radius l^s_{100} for various values of average Ω_b, l^s_{100}/a_{100}, and Λ. Figure 8 corresponds to parameters $\Omega_b = 0.25\ h^{-2}$, $l^s_{100}/a_{100} = 25$, and $\Lambda = 3 \times 10^7$. Figure 10 corresponds to $\Omega_b = 0.025\ h^{-2}$, $l^s_{100}/a_{100} = 20$, and $\Lambda = 1.25 \times 10^6$, whereas, Figure 12 corresponds to parameters $\Omega_b = 0.0125\ h^{-2}$, $l^s_{100}/a_{100} = 20$, and $\Lambda = 1.25 \times 10^6$ and Figure 14 corresponds to parameters $\Omega_b = 0.005\ h^{-2}$, $l^s_{100}/a_{100} = 20$, and $\Lambda = 1.25 \times 10^6$. These figures also give the average ^{7}Be abundance (at $T = 20$ keV and 5 keV) and the average neutron-to-proton ratio (at $T = 20$ keV) as a function of initial fluctuation cell radius l^s_{100}.

Figures 9, 11, and 13 show average nucleosynthesis yields for the same light elements as in Figures 8, 10, 12, and 14, but now presented as a function of initial fluctuation Gaussian width a_{100}. The calculations presented in Figure 9 use $\Omega_b = 0.25\ h^{-2}$, $l^s_{100} = 50$ m, and employ a large density contrast ($\Lambda > 10^6$). The results shown are insensitive to Λ for $\Lambda > 10^6$. Figure 11 corresponds to parameters $\Omega_b = 0.025\ h^{-2}$, $l^s_{100} = 10$ m, and $\Lambda = 1.25 \times 10^7$, whereas Figure 13 corresponds to parameters $\Omega_b = 0.0125\ h^{-2}$, $l^s_{100} = 24$ m, and $\Lambda = 1.25 \times 10^7$.

Several important general trends and results are evident in our IBBN calculations. We find that fluctuations whose cell center separations satisfy $2l^s_{100} \lesssim 1$ m are effectively damped to near-homogeneity by the onset of nuclear freeze-out at $T \approx 100$ keV (see Fig. 3). Comparison of observationally inferred light-element primordial abundances with IBBN calculations can only be used to constrain primordial baryon-to-photon number ratio fluctuations with $2l^s_{100} \gtrsim 1$ m. This conclusion is relatively insensitive to the value of Ω_b and initial values of Λ and a_{100}. Primordial nucleosynthesis in a universe with fluctuations whose separations are smaller than $2l^s_{100} \approx 1$ m is essentially identical to HBBN at the same average Ω_b.

We do not find substantial late-time destruction of ^{7}Be (^{7}Li) as a result of hydrodynamic expansion for any fluctuation characteristics when $\Omega_b \gtrsim 0.025\ h^{-2}$. This is in contrast to suggestions based on simple mixing calculations reported in

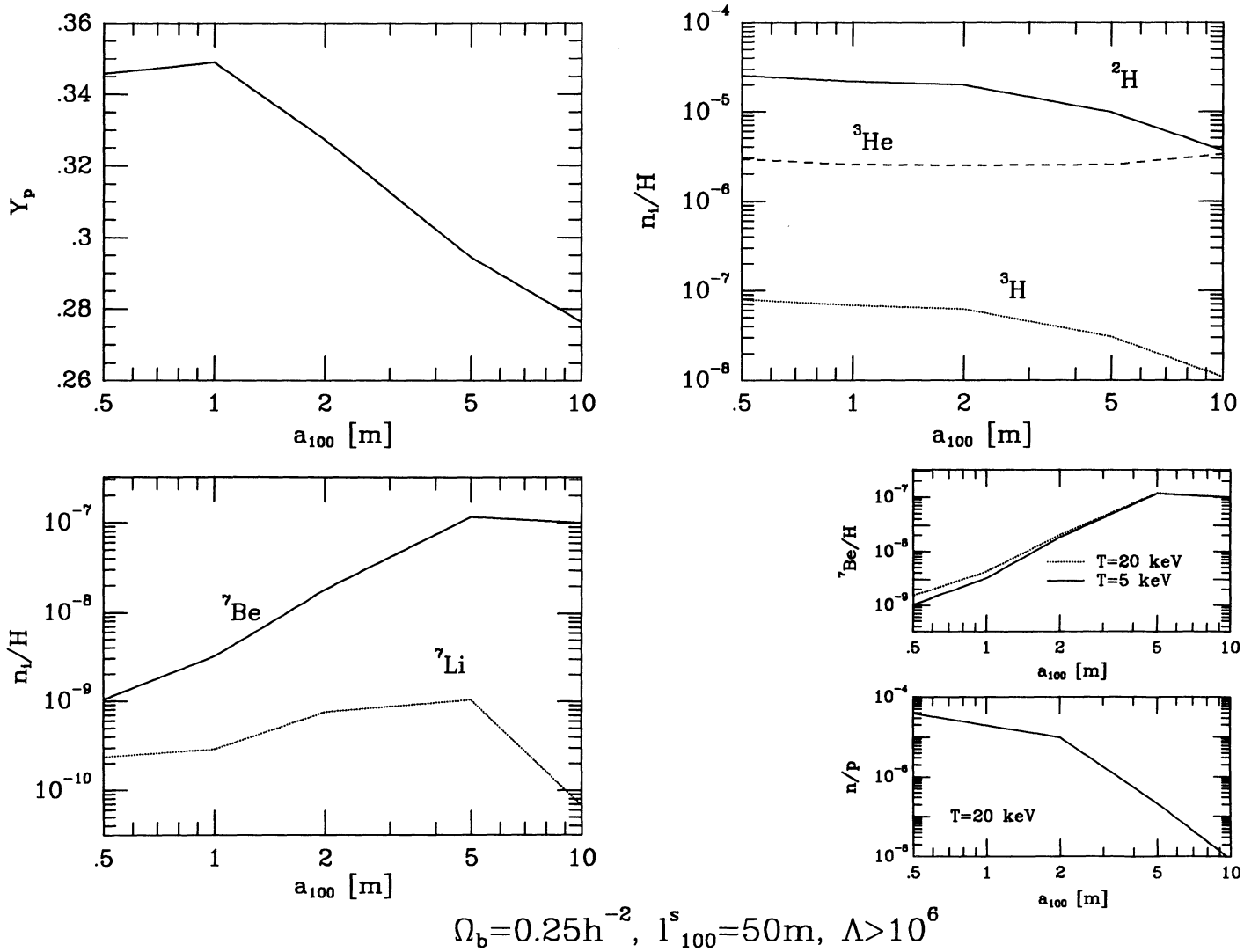

FIG. 9.—Average nucleosynthesis yields are shown as a function of initial fluctuation Gaussian width a_{100} in meters. The panels are as in Fig. 8. These calculations assume average $\Omega_b = 0.25\,h^{-2}$ and initial fluctuation cell radius $l^s_{100} = 50$ m. The initial fluctuation density contrast Λ satisfies $\Lambda \geq 10^6$.

Alcock et al. (1990) and the general schemes for ^{7}Be (^{7}Li) destruction by neutron back-diffusion proposed by Malaney & Fowler (1988) for high average Ω_b universes. Our results imply that any spherically condensed fluctuation characteristics will produce average $^7\mathrm{Li/H} \gtrsim 10^{-9}$ whenever $\Omega_b > 0.013\,h^{-2}$. For some extreme fluctuation characteristics we find $^7\mathrm{Li/H} \approx 10^{-9}$ even for very large Ω_b, but in these cases ^{4}He is overproduced. These considerations force us to surmise that *any* IBBN scenario employing spherically condensed fluctuations will yield essentially the same upper limit on Ω_b as HBBN.

For low Ω_b (see Figs. 12, 13, and 14 where $\Omega_b \leq 0.0125\,h^{-2}$) there can be substantial late-time destruction of ^{7}Li (as ^{7}Be) induced by hydrodynamic expansion. For a narrow range of fluctuation parameters we find $^7\mathrm{Li/H} \approx (1\text{–}3) \times 10^{-10}$, with the ^{2}H, ^{3}He, and ^{4}He yields meeting observational constraints. This low ^{7}Li nucleosynthesis yield is a result of diffusive and hydrodynamic dissipation effects *during* the nucleosynthesis era. It is possible to find fluctuation characteristics (Fig. 14) for which the average ^{4}He mass fraction ($Y_p \approx 0.0225$) is below the minimum from HBBN calculations, but at the cost of a slight overproduction in ^{2}H ($^2\mathrm{H/H} \approx 2.5 \times 10^{-4}$) and ^{7}Li ($^7\mathrm{Li/H} \approx 2.5 \times 10^{-10}$). The recent reestimate of the $^7\mathrm{Li}(^2\mathrm{H}, n)2\alpha$ rate by Boyd, Mitchell, & Meyer (1993) indicates that this process may play an important role in late-time ^{7}Li destruction. We have not incorporated this new rate into our calculations, but its effect may be to decrease our ^{7}Li yields by about a factor of 2. We discuss the effects of dissipation processes and nuclear reaction uncertainties on ^{7}Li IBBN yields in § 3.2.

The studies by Heckler & Hogan (1993) and JF94 show that fluctuations with a broad range of characteristics, but possessing initially large amplitudes, will have convergent evolution. These fluctuations are damped efficiently by neutrino heat conduction at high temperatures ($T \approx 50$–80 MeV) and converge to a generic amplitude ($\eta \sim 10^{-4}$) and shape. This is illustrated in Figure 6.

Fluctuations with these characteristics can produce a substantial mass fraction in elements heavier than $A > 7$ ($X_{A>7} \sim 10^{-9}$). If only a small fraction of the baryons ($\lesssim 2\%$) reside in the high-density cores of these fluctuations, then all light-element abundance constraints can be satisfied. Figure 7 shows the evolution of a fluctuation with the appropriate characteristics. Jedamzik et al. (1993) have used an extended nuclear

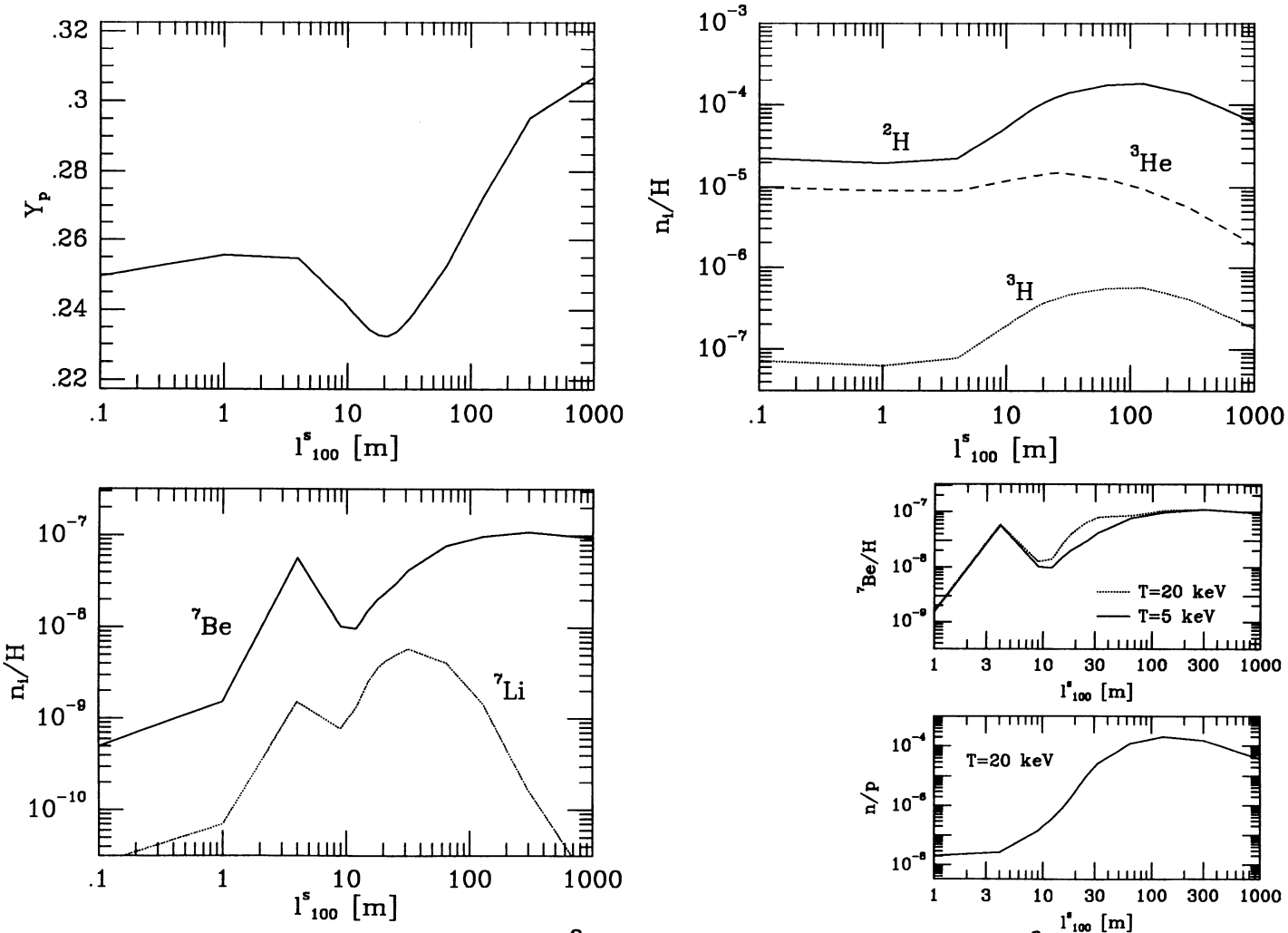

FIG. 10.—Same as Fig. 8, but with average $\Omega_b = 0.025\ h^{-2}$ and initial fluctuation parameters $\Lambda = 1.25 \times 10^6$ and $l^s_{100}/a_{100} = 20$

reaction network to investigate the abundance pattern which emerges from the nucleosynthesis process in such fluctuations. They find that intermediate-mass nuclei on the proton-rich side of the valley of beta stability can be significantly produced as a possible observable signature of such inhomogeneities.

Our calculations show that late-time *r*-process of heavy nuclides associated with the neutron-rich low-density regions of fluctuation cells (Applegate 1988; Rauscher et al. 1993) is very unlikely. We find that neutron back-diffusion effectively eliminates neutron-rich low-density environments before the onset of an *r*-process is possible.

Our investigation shows that it is remarkably difficult to reconcile inhomogeneous big bang nucleosynthesis yields with observationally inferred primordial light-element abundances. In fact, only very narrow ranges of fluctuation characteristics can give nuclear abundances which satisfy observational constraints. In the following subsections we discuss some specific features of IBBN production of ^{4}He, ^{7}Li, ^{2}H, and ^{3}He.

3.1. ^{4}He

The production of ^{4}He in IBBN models can be sensitive to neutron back-diffusion but is influenced very little by late-time hydrodynamic fluctuation damping. In the proton-rich high-density core regions of fluctuation cells ^{4}He is synthesized in essentially the same manner as in HBBN. In these regions nearly all of the neutrons which remain at the epoch of nuclear statistical equilibrium (NSE) freeze-out are incorporated into alpha particles. This implies that the neutron number density in these regions serves as a bottleneck for ^{4}He production. Substantial ^{4}He production in the high-density cores in our models occurs at temperatures between $T \approx 300$ keV and $T \approx 100$ keV, depending upon the fluctuation characteristics.

The low-density outer regions of fluctuation cells can be neutron-rich. The synthesis of ^{4}He in these regions generally proceeds at later times and lower temperatures than in higher density proton-rich regimes. Significant ^{4}He synthesis in these regions typically occurs for temperatures $T \sim 50$ keV.

The high- and low-density regions in fluctuation cells may or may not be efficiently coupled by neutron diffusion. Neutrons cannot readily diffuse out of high-density regions if fluctuation centers have separations ($2l^s_{100}$) which are very large compared with the neutron diffusion length at NSE freeze-out and have smaller values of l^s_{100}/a_{100}. The result is ^{4}He overproduction. This trend is evident in Figure 4. Likewise, if fluctuations have values of $2l^s_{100}$ which are small compared with the neutron

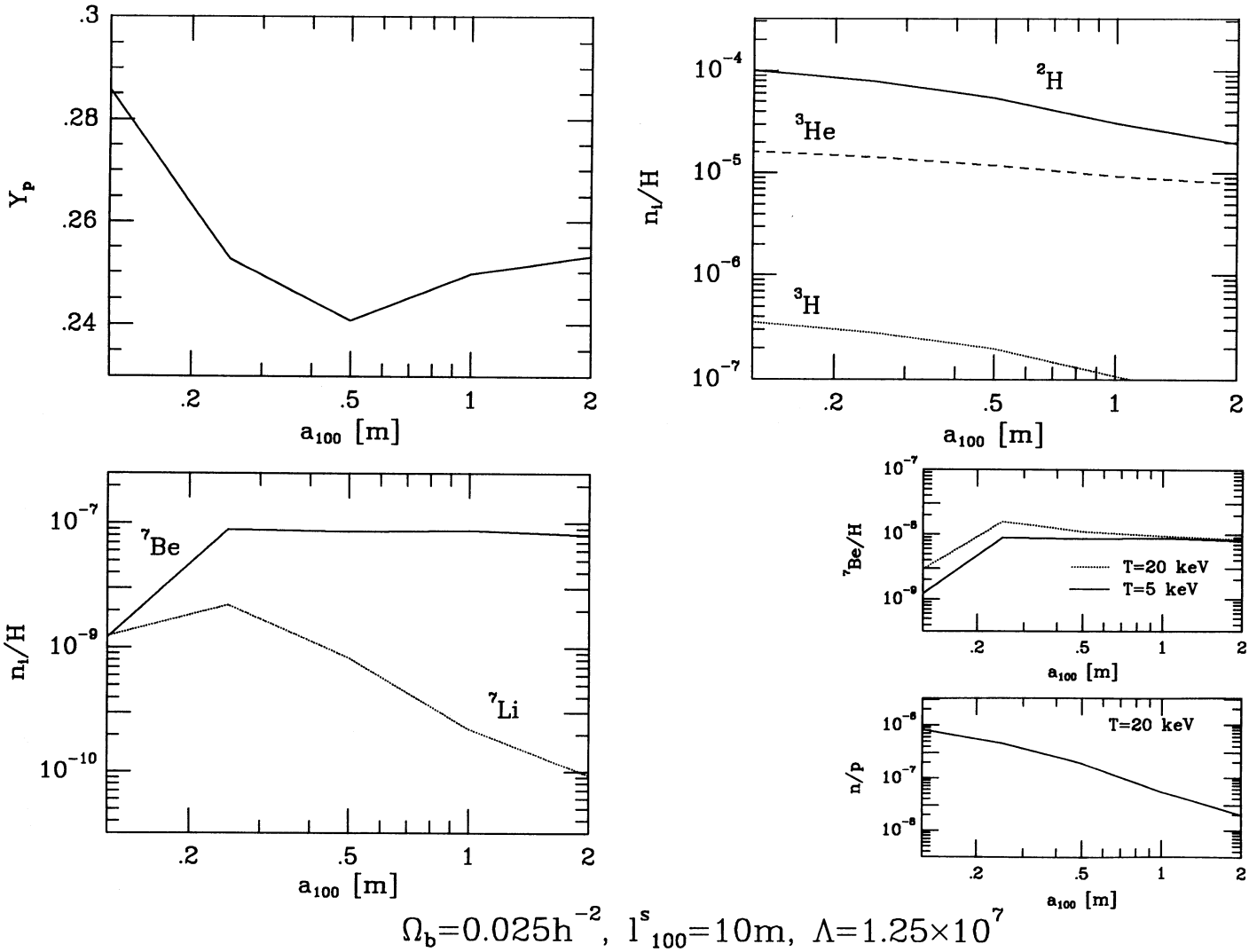

FIG. 11.—Same as Fig. 9, but with average $\Omega_b = 0.025\ h^{-2}$ and initial fluctuation parameters $\Lambda = 1.25 \times 10^7$ and $l^s_{100} = 10$ m

diffusion length, then efficient back-diffusion of neutrons from low-density neutron-rich regions into higher density zones takes place. This back-diffusion is driven by the gradient in neutron number density which develops as neutrons are consumed in the higher density regions. Most neutrons which diffuse back toward high-density zones are incorporated into alpha particles. The result can again lead to ^{4}He overproduction. This is evident in Figure 5, where back-diffusion–driven ^{4}He production is dominant.

The average nucleosynthesis yield of ^{4}He can be a minimum when the value of $2l^s_{100}$ is roughly the same as the neutron diffusion length at the epoch of NSE freeze-out. This ^{4}He "dip" is a general feature of IBBN models (Alcock, Fuller, & Mathews 1987; Kurki-Suonio et al. 1988; Mathews et al. 1990). Figures 10, 12, and 14 give good examples of the ^{4}He dip. Note that the position of the dip depends upon fluctuation characteristics to some extent. In our studies the dip occurs for l^s_{100} between 20 and 50 m and becomes deeper and more pronounced for lower values of Ω_b.

Photon diffusive damping and hydrodynamic expansion of fluctuations only become significant after the epoch of $e^\pm$ annihilation. The photon opacity depends sensitively on the number density of electrons and positrons. Pairs make an appreciable contribution to the total electron number density until the temperature falls below about $T \approx 30$ keV to $T \approx 20$ keV. Hydrodynamic effects are important when the photon mean free path becomes comparable to the size of the high-density core regions of fluctuations. In our studies this typically occurs in approximate coincidence with the end of $e^\pm$ pair domination of the electron number density. At these temperatures ^{4}He production is inhibited by the Coulomb barriers of key reaction rates. This conclusion does not apply to late-time ^{7}Be (^{7}Li) destruction or ^{2}H production.

3.2. ^{7}Li

In IBBN models ^{7}Li can be produced directly by ^{3}H(α, γ)^{7}Li in neutron-rich low-density conditions, or as ^{7}Be via ^{3}He(α, γ)^{7}Be in high-density regions. The ^{7}Be is converted to ^{7}Li by ^{7}Be(e^-, ν_e)^{7}Li on a timescale long compared to nucleosynthesis times.

Most of the total average ^{7}Li yield comes from the ^{7}Be production channel whenever fluctuations have large Λ and small l^s_{100}/a_{100}. This is evident in Figures 4 and 6. These figures show that a significant fraction of the ^{7}Be can be produced in a

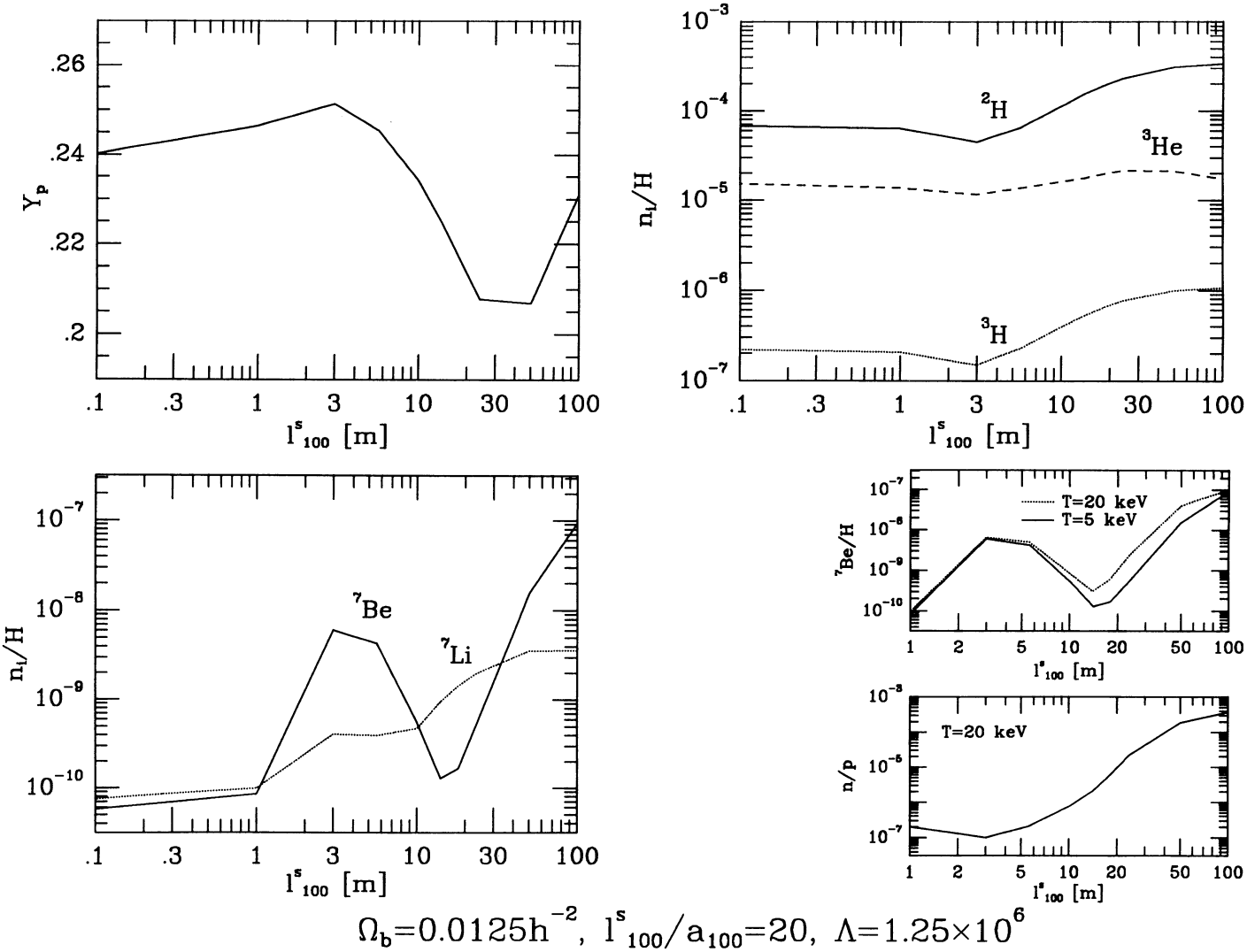

FIG. 12.—Same as Fig. 8, but with average $\Omega_b = 0.0125\ h^{-2}$ and initial fluctuation parameters $\Lambda = 1.25 \times 10^6$ and $l^s_{100}/a_{100} = 20$

spherical shell at the edge of the high-density core region in a fluctuation cell. This spatial distribution of ^{7}Be makes the average nucleosynthesis yields of ^{7}Li in IBBN models particularly sensitive to back-diffusion (Malaney & Fowler 1988). Back-diffusion of neutrons into the ^{7}Be shell can induce the reaction sequence ^{7}Be(n, p)^{7}Li(p, α)α. These reactions can reduce the ultimate average ^{7}Li nucleosynthesis yield in IBBN models. This destruction process can be very effective due to the extremely large value of the ^{7}Be neutron capture cross section.

Hydrodynamic expansion of the high-density core regions of fluctuations can effectively enhance the back-diffusion of neutrons and the associated destruction of ^{7}Be. Alcock et al. (1990) modeled the fluctuation expansion by instantaneously mixing high- and low-density material at temperature T_m. This mixing temperature was taken to coincide with the beginning of rapid photon-drag–limited expansion. They found, however, that the efficiency of the ^{7}Be destruction process was sensitive to the choice of T_m and, hence, to particular fluctuation characteristics.

In Figure 15 we compare the yields from our hydrodynamic calculations with simple mixing approximations. In this figure we plot the average ^{7}Be/H in a fluctuation cell against cosmic temperature. The initial fluctuation parameters employed in this calculation are $\Lambda = 2 \times 10^7$, $l^s_{100} = 50$ m, and $l^s_{100}/a_{100} = 20$. In this calculation we assumed a large value for the baryonic density, corresponding to $\Omega_b = 0.25\ h^{-2}$. This figure shows a fully hydrodynamic calculation result (*solid line*), a case where hydrodynamic expansion times are decreased by a factor of 20 (*dotted line*), and three schematic mixing calculations where all nuclear species and densities are instantaneously homogenized at the indicated value of T_m. The dash-dot line corresponds to a calculation with mixing at $T = 27$ keV in which reaction rate set I is employed (Table 1). The short-dashed and long-dashed curves correspond to mixing calculations with $T_m = 20$ keV in which we used reaction rate sets I and II, respectively. Table 1 lists reaction rates for $p(n, \gamma)^2$H and ^{7}Be(n, p)^{7}Li taken from Smith et al. (1993), Mathews et al. (1990), and Fowler (1993). The Smith et al. (1993) rates constitute reaction rate set I, while the Matthews et al. (1990) and

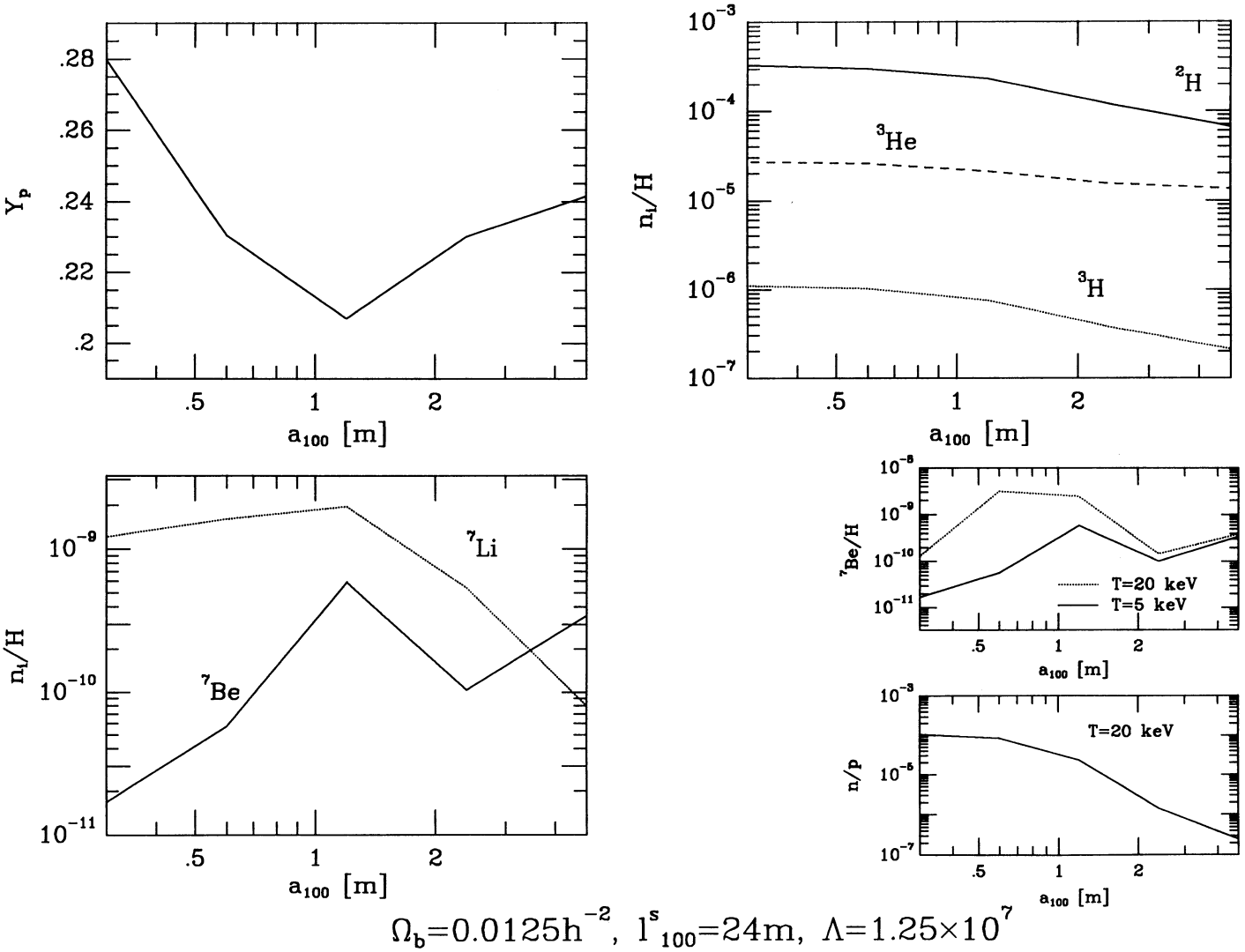

FIG. 13.—Same as Fig. 9, but with average $\Omega_b = 0.0125\ h^{-2}$ and initial fluctuation parameters $\Lambda = 1.25 \times 10^7$ and $l^s_{100} = 24$ m

TABLE 1

NUCLEAR REACTION RATE SETS

Reaction	Set	Reference	Reaction Rate λ[a] ($cm^3\ s^{-1}\ mol^{-1}$)
$p(n,\gamma)^2H$	I	Smith et al. 1993	$4.2742 \times 10^4(1 - 0.8504T_9^{1/2} = 0.4895T_9 - 0.09623T_9^{3/2} + 8.471 \times 10^{-3}T_9^2 - 2.80 \times 10^{-4}T_9^{5/2})$
	II	Mathews et al. 1990	$4.40 \times 10^4(1 - 0.860T_9^{1/2} + 0.429T_9 - 0.09623T_9^{3/2} + 8.471 \times 10^{-3}T_9^2 - 2.80 \times 10^{-4}T_9^{5/2}$
	III	Caughlan & Fowler 1988	$4.40 \times 10^4(1 - 0.860T_9^{1/2} + 0.429T_9 - 0.09623T_9^{3/2} + 8.471 \times 10^{-3}T_9^2 - 2.80 \times 10^{-4}T_9^{5/2})$
$^7Be(n,p)^7Li$	I	Smith et al. 1993	$2.675 \times 10^9(1 - 0.560T_9^{1/2} + 0.179T_9 - 0.0283T_9^{3/2} + 2.214 \times 10^{-3}T_9^2 - 6.851 \times 10^{-5}T_9^{5/2} + 9.391 \times 10^8(1 + 13.076)^{-3/2} + 4.467 \times 10^7 \exp(-0.07486/T_9))$
	II	Mathews et al. 1990	$6.76 \times 10^9(1 - 0.903T_9^{1/2} + 0.218T_9)$
	III	Fowler 1993	$5.14 \times 10^9 \exp(-1.167T_9^{1/3})$

[a] T_9 = temperature in units of 10^9 K.

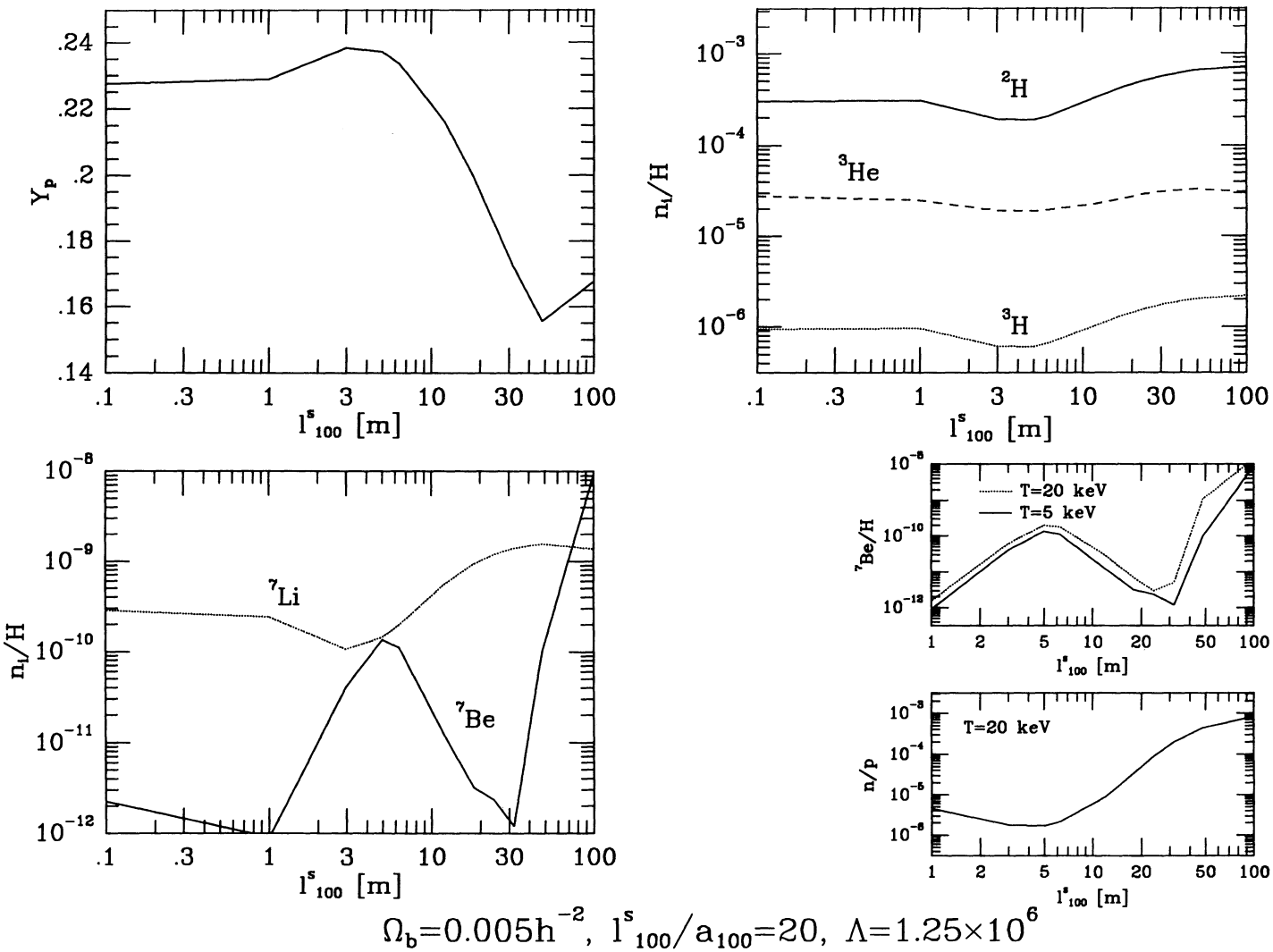

FIG. 14.—Same as Fig. 8, but with average $\Omega_b = 0.005\ h^{-2}$ and initial fluctuation parameters $\Lambda = 1.25 \times 10^6$ and $l^s_{100}/a_{100} = 20$

Fowler (1993) rates comprise reaction rate sets II and III, respectively. Our hydrodynamic calculations employ reaction rate set II.

The mixing calculations shown in Figure 15 reproduce the results found in Alcock et al. (1990). We note, however, that our realistic hydrodynamic calculations do not show the large amounts of ^{7}Be destruction obtained in mixing calculations. Even if we artificially increase the expansion rate of exploding fluctuations by a factor of 20, this conclusion would not change. Figure 15 shows that ^{7}Be late-time destruction can be sensitive to the nuclear reaction rates employed in the calculations. This fact can be important for IBBN calculations at low Ω_b, where ^{7}Be destruction is more significant.

General considerations of neutron numbers and reaction cross sections can be used to understand the requirements for significant ^{7}Be destruction. Two processes which remove neutrons compete with the ^{7}Be$(n, p)^7$Li destruction channel: radiative neutron capture by protons, and free neutron decay. Neutrons diffusing back into high-density regions will be consumed principally by either $p(n, \gamma)^2$H or ^{7}Be$(n, p)^7$Li. Comparing the reaction rates for these processes, we find

$$\left(\frac{1}{y_n}\frac{dy_n}{dt}\bigg|_{pn}\right)\Big/\left(\frac{1}{y_n}\frac{dy_n}{dt}\bigg|_{n\mathrm{Be}}\right) = \frac{\lambda_{pn}\, y_{\mathrm{H}}}{\lambda_{n\mathrm{Be}}\, y_{^7\mathrm{Be}}} \approx 6 \times 10^{-6}\, \frac{y y_{\mathrm{H}}}{y_{^7\mathrm{Be}}}\,, \quad (5)$$

where y_n, y_{H}, and $y_{^7\mathrm{Be}}$ are the neutron, proton, and ^{7}Be number fractions relative to hydrogen, respectively. With this notation $y_{\mathrm{H}} = 1$. In equation (5) λ_{pn} is the reaction rate for $p(n, \gamma)^2$H, while $\lambda_{n\mathrm{Be}}$ is the rate for ^{7}Be$(n, p)^7$Li. A ^{7}Be abundance of $y_{^7\mathrm{Be}} \sim 10^{-8}$ is typical for the epochs where rapid hydrodynamic expansion is likely. From this and equation (5) we see that only about one in 600 neutrons will be captured on ^{7}Be. We conclude that efficient ^{7}Be destruction would require that roughly 600 neutrons per ^{7}Be nucleus be delivered to the high-density core regions of fluctuations by neutron back-diffusion. This neutron number requirement might be lowered somewhat if the ^{7}Be resides in a narrow shell on the edge of the high-density region. Requiring 600 neutrons per ^{7}Be nucleus in order to have efficient ^{7}Be destruction implies that the average neutron abundance has to exceed $y_n \gtrsim 600 y_{^7\mathrm{Be}} \approx 6 \times 10^{-6} \sim 10^{-5}$. This condition is independent of the ^{7}Be abundance. Free neutron decay will reduce y_n below 10^{-5} unless hydrodynamic expansion and the associated enhancement in the neutron back-diffusion rate occur early enough ($T \gtrsim 20$ keV).

Figures 10 and 12 illustrate how the ^{7}Be/H ($y_{^7\mathrm{Be}}$) and neutron-to-proton ratios depend on l^s_{100} for representative fluctuation characteristics. It is clear from these figures that $y_n > 10^{-5}$ when $l^s_{100} \gtrsim 10$ m at an epoch where $T = 20$ keV. We note that appreciable ^{7}Be destruction occurs for l^s_{100}

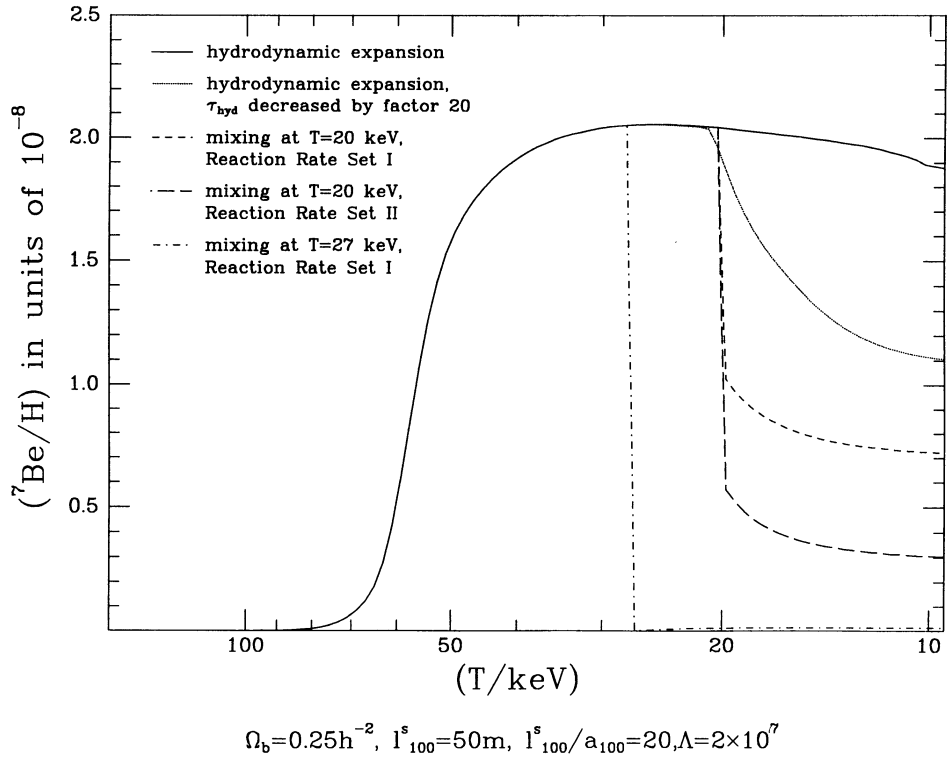

FIG. 15.—Average ^{7}Be/H abundance (in units of 10^{-8}) is shown as a function of cosmic temperature T in keV for five calculations. Correspondence between individual curves and calculation techniques is as indicated in the key. All results employ a fluctuation with parameters $\Lambda = 2 \times 10^7$, $l^s_{100} = 50$ m, $l^s_{100}/a_{100} = 20$, and average $\Omega_b = 0.25\,h^{-2}$.

between 10 and 50 m, as expected. For $l^s_{100} > 50$ m we find $y_n > 10^{-5}$, but late-time expansion is inefficient and there is little ^{7}Be destruction.

The efficiency of ^{7}Be destruction associated with late-time hydrodynamic disassembly of fluctuations depends upon the average value of Ω_b employed in the calculations. In Figure 16 we show the ^{7}Li and ^{7}Be average abundances as a function of cosmic temperature derived from calculations with hydrodynamic expansion (*solid curve*) and without it (*dashed curves*). The fluctuation parameters here are the same as in Figure 10, except that l^s_{100} is fixed at $l^s_{100} = 12$ m. These calculations employ a large value for the average baryon density, $\Omega_b = 0.025\ h^{-2}$. The overall ^{7}Li yield in this case is dominated by ^{7}Be production in higher density regions. We see that hydrodynamic effects induce a decrease in ^{7}Be/H by a factor of 1.5. Note that a small amount of ^{7}Li is produced in the course of the ^{7}Be destruction. This is because the ^{7}Li$(p, \alpha)\alpha$ rate is not completely effective in destroying ^{7}Li in the high-density zones at low temperatures.

For low average Ω_b the ^{7}Be destruction caused by hydrodynamic fluctuation damping can be significant. Figure 17 shows ^{7}Li and ^{7}Be average abundances as a function of temperature for calculations with and without hydrodynamic effects. The notation in this figure is the same as in Figure 16. An average baryon density of $\Omega_b = 0.0125\ h^{-2}$ was used in the calculations whose results are shown in Figure 17. This Ω_b is a factor of 2 lower than that employed in the calculation shown in Figure 16. The fluctuation parameters employed for Figure 17 are the same as those in Figure 16, except for an insignificant difference in l^s_{100}. In the low Ω_b calculation we see that ^{7}Be is destroyed by approximately a factor of 5. However, in this case most of the final average ^{7}Li yield comes from direct ^{7}Li production in low-density regions.

We find that lower average Ω_b leads to an earlier onset time and an enhanced vigor for hydrodynamic fluctuation dissipation. These effects result in increased ^{7}Be destruction. The onset of rapid hydrodynamic evolution occurs when the

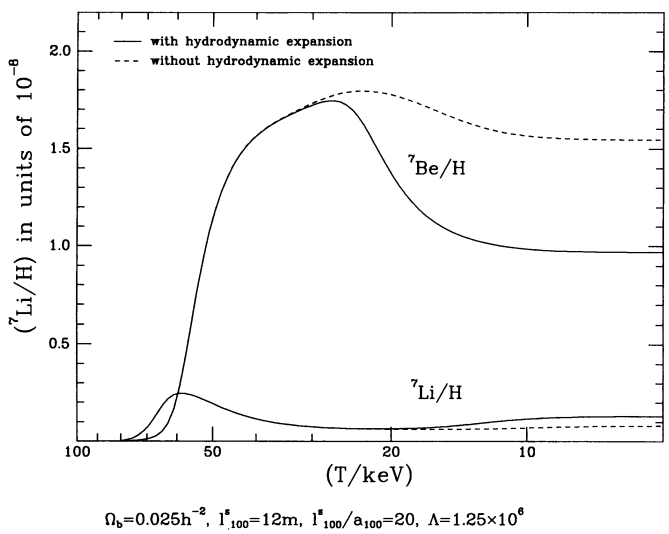

FIG. 16.—^{7}Li/H and ^{7}Be/H in units of 10^{-8} are plotted against temperature T in keV. Solid lines give results for a calculation with full hydrodynamic effects. Dashed lines are for a calculation without hydrodynamic expansion effects. The calculations employ $\Omega_b = 0.025\ h^{-2}$ and have initial fluctuation parameters $\Lambda = 1.25 \times 10^6$, $l^s_{100} = 12$ m, and $l^s_{100}/a_{100} = 20$.

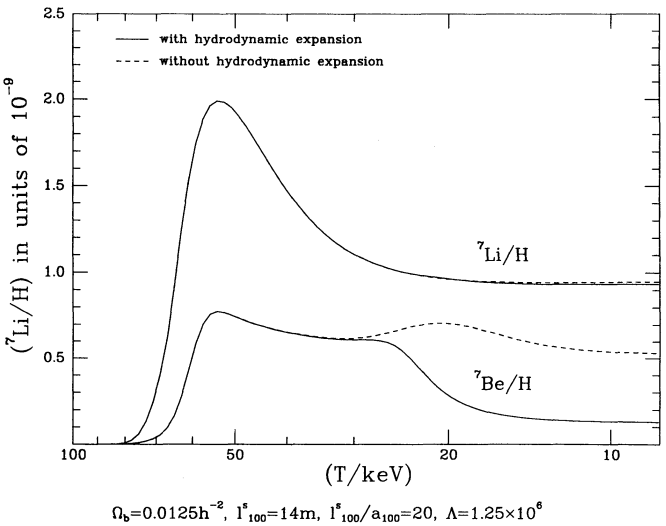

Ω_b=0.0125h^{-2}, l^s_{100}=14m, l^s_{100}/a_{100}=20, Λ=1.25×10^6

FIG. 17.—Same as Fig. 16, but for calculations with $\Omega_b = 0.0125\ h^{-2}$. Fluctuation parameters are the same as in Fig. 16, except that $l^s_{100} = 14$ m.

comoving photon mean free path, l^γ_{100}, exceeds the comoving length scale associated with the high-density core region of a fluctuation cell, L^H_{100}. Our calculations show that

$$\left(\frac{l^\gamma_{100}}{L^H_{100}}\right) \approx 0.4(\Omega^H_{\rm eff})^{-1}\left(\frac{T}{20\ {\rm keV}}\right)^{-2}\left(\frac{L^H_{100}}{1\ {\rm m}}\right)^{-1}, \qquad (6)$$

where $\Omega^H_{\rm eff}$ is the effective baryon density in the core region divided by the closure density. For given fluctuation characteristics a lower average Ω_b will result in a smaller $\Omega^H_{\rm eff}$ and, therefore, an earlier onset time for hydrodynamic expansion. A smaller value for L^H_{100} produces a similar effect. Figure 13 illustrates these trends. In interpreting this figure, it helps to note that small a_{100} tends to be associated with smaller values for L^H_{100}. This figure shows nearly a two order of magnitude destruction of ^{7}Be for small a_{100}.

3.3. *Deuterium and* ^{3}He

The nucleosynthesis yield of ^{3}He in our IBBN study is relatively insensitive to fluctuation parameters. This is because ^{3}He is produced in both high- and low-density regions of a fluctuation cell. As is evident from Figures 8–14, we find a ^{3}He abundance relative to hydrogen of $2 \times 10^{-6} < y_{^3{\rm He}} < 3 \times 10^{-5}$ in our survey. Large ^{3}He abundances are produced only in low average Ω_b universes.

Deuterium is produced only in relatively low-density regions of fluctuation cells. We find that average ^{2}H abundance yields are sensitive to l^s_{100}, l^s_{100}/a_{100}, and Λ. There is a rather firm lower bound on the primordial ^{2}H abundance of $y_{^2{\rm H}} \gtrsim 1.8 \times 10^{-5}$ (Walker et al. 1991). This limit presupposes no significant non–big bang source of ^{2}H (see the discussion in Gnedin & Ostriker 1992). Dearborn, Schramm, & Steigman (1986) derive an upper bound on the sum of ^{2}H and ^{3}He of $(y_{^2{\rm H}} + y_{^3{\rm He}}) \lesssim 9 \times 10^{-5}$. We find that IBBN models with low average Ω_b frequently produce ^{2}H yields which exceed this upper limit.

4. CONCLUSIONS

We have studied the primordial nucleosynthesis process for universes with spherically condensed high-amplitude baryon-to-photon fluctuations. Unlike previous efforts to investigate this problem, our numerical calculations couple nuclear reactions with all important diffusive and hydrodynamic fluctuation dissipation mechanisms. These hydrodynamic effects can be important for determining the final light-element abundance yields in our IBBN models.

We find considerable hydrodynamic-expansion–induced destruction of ^{7}Be (^{7}Li) only for IBBN models which employ low average Ω_b ($\Omega_b \lesssim 0.013\ h^{-2}$). At higher Ω_b there is little hydrodynamic influence on the ^{7}Li yield. Our results show that it is not possible to invoke spherically condensed fluctuations to circumvent the upper bound on Ω_b derived from HBBN.

Even for low Ω_b, the only way to reconcile IBBN abundance yields with observational limits is to fine-tune fluctuation parameters. This leads to the conclusion that any process in the early universe which generates nonlinear fluctuations prior to the epoch where $T \approx 100$ keV may be subject to nucleosynthesis constraints.

We wish to thank C. R. Alcock, W. A. Fowler, B. S. Meyer, L. H. Kawano, and M. S. Smith for useful conversations and helpful suggestions. This work was supported in part by NSF grant PHY91-21623 and IGPP LLNL grant 93-22. It was also performed in part under the auspices of the US Department of Energy by the Lawrence Livermore National Laboratory under contract number W-7405-ENG-48 and DoE Nuclear Theory grant SF-ENG-48.

REFERENCES

Alcock, C. R., Dearborn, D. S. P., Fuller, G. M., Mathews, G. J., & Meyer, B. 1990, Phys. Rev. Lett., 64, 2607
Alcock, C. R., Fuller, G. M., & Mathews, G. J. 1987, ApJ, 320, 439
Applegate, J. H. 1988, Phys. Rep., 163, 141
Applegate, J. H., Hogan, C. J., & Scherrer, R. J. 1987, Phys. Rev. D, 35, 1151
Boyd, R. N., Mitchell, C. A., & Meyer, B. S. 1993, Phys. Rev. C, 47, 3269
Caughlan, G. R., & Fowler, W. A. 1988, Atomic Data Nucl. Data, 40, 291
Dearborn, D. S. P., Schramm, D. N., & Steigman, G. 1986, ApJ, 302, 35
Dolgov, A., & Silk, J. 1993, Phys. Rev. D, 47, 4244
Epstein, R. I., & Petrosian, V. 1975, ApJ, 197, 281
Fowler, W. A. 1993, Phys. Rep., 227, 313
Fuller, G. M., Mathews, G. J., & Alcock, C. R. 1988, Phys. Rev. D, 37, 1380
Gnedin, N. Y., & Ostriker, J. P. 1992, ApJ, 400, 1
Heckler, A., & Hogan, C. J. 1993, Phys. Rev. D, 47, 4256
Jedamzik, K., & Fuller, G. M. 1994, ApJ, 422, 33 (JF94)
Jedamzik, K., Fuller, G. M., Mathews, G. J., & Kajino, T. 1994, ApJ, in press
Kawano, L. H. 1992, Fermilab-Pub-92/04-A, preprint
Kolb, E. W., & Turner, M. S. 1990, The Early Universe (Reading: Addison-Wesley)
Kurki-Suonio, H., & Matzner, R. 1989, Phys. Rev. D, 39, 1046
———. 1990, Phys. Rev. D, 42, 1047
Kurki-Suonio, H., Matzner, R. A., Centrella, J., Rothman, T., & Wilson, J. R. 1988, Phys. Rev. D, 38, 1091
Kurki-Suonio, H., Matzner, R. A., Olive, K. A., & Schramm, D. N. 1990, ApJ, 353, 406
Malaney, R. A., & Fowler, W. A. 1988, ApJ, 333, 14
Malaney, R. A., & Mathews, G. J. 1993, Phys. Rep., 229, 145
Mathews, G. J., Meyer, B. S., Alcock, C. R., & Fuller, G. M. 1990, ApJ, 358, 36
Meyer, B. S., Alcock, C. R., Mathews, G. J., & Fuller, G. M. 1991, Phys. Rev. D, 43, 1079
Rauscher, T., Applegate, J. H., Cowan, J. J., Thielemann, F. K., & Wiescher, M. 1993, ApJ, submitted
Schramm, D. N., & Wagoner, R. V. 1977, Ann. Rev. Nucl. Part. Sci., 27, 37
Smith, M. S., Kawano, L. H., & Malaney, R. A. 1993, ApJS, 85, 219
Terasawa, N., & Sato, K. 1989a, Prog. Theor. Phys., 81, 254
———. 1989b, Phys. Rev. D, 39, 2893
———. 1989c, Prog. Theor. Phys., 81, 1085
———. 1990, ApJ, 362, L47
Thomas, D., Schramm, D. N., Olive, K. A., Mathews, G. J., Meyer, B. S., & Fields, B. D. 1994, ApJ, submitted
Wagoner, R. V. 1973, ApJ, 179, 343
Wagoner, R. V., Fowler, W. A., & Hoyle, F. 1967, ApJ, 148, 3
Walker, T. P., Steigman, G., Schramm, D. N., Olive, K. A., & Kang, H. 1991, ApJ, 376, 51
Yang, J., Turner, M. S., Steigman, G., Schramm, D. N., & Olive, K. A. 1984, ApJ, 281, 493
Yokoyama, J., & Suto, Y. 1991, ApJ, 379, 427